Rev. Adv. Mater. Sci. 46 (2016) 53-69

NANOCRYSTAL FORMATION IN LIGHT METALLIC GLASSES AT HEATING AND DEFORMATION

A. Aronin[1], A. Budchenko[1], D. Matveev[1], E. Pershina[1], V. Tkatch[2] and G. Abrosimova[1]

[1]Institute of Solid State Physics RAS, Chernogolovka, Russia
[2]Donetsk Physics and Engineering Institute of NAS of Ukraine, Donetsk, Ukraine

Received: April 23, 2016

Abstract. Structure evolution of amorphous alloys at heat treatment and deformation is discussed. Amorphous structure change before crystallization is considered for Al-, Ni-, Fe-, Zr-based systems. Property change with structure evolution is discussed as well. Nanocrystal formation in light metallic glasses is studied at heating and deformation. The sizes of the nanocrystals forming during plastic deformation were found to be smaller than those of the nanocrystals forming on thermal treatment. The sizes of the nanocrystals do not change (Al-Ni-Gd, Al-Y) or change only slightly (Al-Ni-La) with increasing degree of plastic deformation whilst their volume content increases and the fraction of nanocrystals in the deformed samples is larger than that in the samples subjected to thermal treatment. Using combined treatment (plastic deformation + annealing) was observed to result in intermediate nanocrystals size.

1. INTRODUCTION

High technology development is based on fundamental research. Development of principles of producing novel materials is guided by the knowledge of the basic processes that condition formation of particular materials, structural correlation and corresponding physicochemical properties. Given the fact that most physicochemical properties are structure-sensitive, understanding of the processes providing the basis of formation of any particular structure is of crucial significance. Among such novel materials are nanocrystalline metallic materials. Nanocrystalline structure can be obtained by different techniques [1-5], one of the main being controlled crystallization of amorphous alloys which enables formation of composite structure consisting of nanocrystals that are randomly arranged in the amorphous matrix. One of the advantages of the method of producing nanocrystalline structure by partial crystallization of amorphous alloys is the possibility to control nanostructure parameters and, hence, their physical properties by varying conditions of thermal treatment. For instance, the optimal combination of high strength and plasticity of Al-TM-RE alloys is achieved in nanocomposite structures with certain sizes of Al nanocrystals and their volume fraction.

Metallic alloys with an amorphous - nanocrystalline structure (amorphous - nanocrystalline materials - ANCM) are now among the most promising materials with a complex of high physical-mechanical properties. Application of this class of materials is now mainly due to the high magnetic characteristics of iron-based ANCM. Yet, along with soft magnetic ANCM, light and high strength aluminum-based ANCM is also promising since the values of ultimate strength of aluminum-based alloys with 6-15% of transition metal (Fe, Co, Ni) and several percent of rare earth metal reaches

Corresponding author: A. Aronin, e-mail: aronin@issp.ac.ru

1.6 GPa [5,6]. It should be emphasized that these strength values are comparable to those of tool steel whilst the specific weight of aluminum-based alloys is approximately 2.5 times lower. Such alloy characteristics are attractive for practical applications. Similar materials, however, were obtained at the end of the 20th century but they have not found any important application yet, which is largely due to their high brittleness. As a rule, ANCM is produced by controlled crystallization of the amorphous phase on heating or isothermal annealing. The first crystallization stage (primary crystallization) gives rise to aluminum nanocrystals, their fraction depends on alloy composition and is within 20%-30%. Formation of nanocrystals proceeds by the diffusion mechanism as composition of nanocrystals differs from that of the initial amorphous matrix [7-10]. The mechanical properties of such a double phase nanocomposite system should be determined by the mechanical characteristics (yield strength, elastic modules, plasticity, etc.) both of structural specific features of nanocrystals and the amorphous phase as well as morphology of nanocrystals and their matrix arrangement [11].

A new technique for producing nanostructures has been recently developed: nanocrystallization of amorphous alloys subjected to deformation. In both cases, thermal treatment and deformation, the process of nanocrystal formation is determined by the higher parameters of diffusion mass transfer. The nucleation mechanism of nanocrystals is now under investigation, yet, no final solution has been found, for instance, the role of shear bands is not yet clear [12]. It should be noted that controlled crystallization of amorphous alloys under heating and deformation conditions results in formation of nanostructures with different parameters [13-18]. Now there are a lot of data on sizes and morphology of nanocrystals produced by different methods [19-27].

The nanocrystal size increases either due to increasing temperature of thermal treatment or changes in amorphous alloy matrix structure in places of deformation-induced nanocrystal formation (in the vicinity of shear bands). Deformation may also cause changes in the chemical composition of the amorphous alloy regions of localized plastic deformation. Such deformation-induced changes of the amorphous matrix should involve changes in the number of nucleation centers and, hence, affect the structural parameters of the forming phase, which, in turn, brings about changes in the conditions of nanocrystal nucleation and growth. Since mechanical properties are structure-sensitive, production of materials with specified properties including aluminum-based ANCM requires knowledge of regularities and mechanisms of ANCM formation followed by establishment of structure-property correlation.

Let us consider the changes that may occur in the amorphous structure during heat treatment and deformation.

2. CHANGES IN THE AMORPHOUS STRUCTURE DURING THE HEAT TREATMENT

Any approach to the description of the amorphous structure suggests that it is a homogeneous isotropic structure. In fact, it was turned out that the structure of the amorphous phase in alloys can not always be uniform and isotropic. It was shown in a lot of studies that the structure of amorphous alloys are not uniform ($Pd_{74}Au_8Si_{18}$ [28], $Pd_{40.5}Ni_{40.5}P_{19}$ [29], $Be_{40}Ti_{24}Zr_{36}$ [30]).This is clearly seen in X-ray diffraction patterns. Double halo in the X-ray diffraction patterns was observed for amorphous Al-Si-X and Al-Ge-X (X = Ti, Zr, V, W, Mn, Fe, Co, Ni, Cu, Cr, Nb, Mo) alloys [31-33]. Heterogeneities in the structure were found after various external influences: heat treatment, irradiation, and others. For example, as-prepared amorphous Pd-Au-Si alloy is uniform, but after annealing at 400 °C separation into regions with different elemental composition was observed [34]; in study of amorphous $(Mo_{0.6}Ru_{0.4})_{100-x}B_x$ alloy, the formation of chemical segregation was found before the crystallization [35]. Thus, the crystallization is often preceded by of the amorphous phase separation into regions of different chemical composition and different short-range order, i.e. the formation of two or more amorphous phases [36-40]. These phases do not separated by sharp interface, and the transformation may exhibit spinodal decomposition characteristics [28]. In studying the structure of Pd-Au-Si alloys [34] amorphous phase separation was found to depend on chemical composition; and the tendency to phase separation increases with the concentration of gold.

Evolution of the amorphous phase depends on temperature. Heating and annealing of the metallic glasses can be performed in two different temperature ranges: above and below the glass transition temperature T_g. Above the glass transition temperature the amorphous phase is in a supercooled liquid state, below glass transition temperature it is in fact the amorphous state. It is known that when passing through the glass transition temperature T_g material properties change sharply (viscosity, enthalpy, heat capacity, specific volume, and others.).

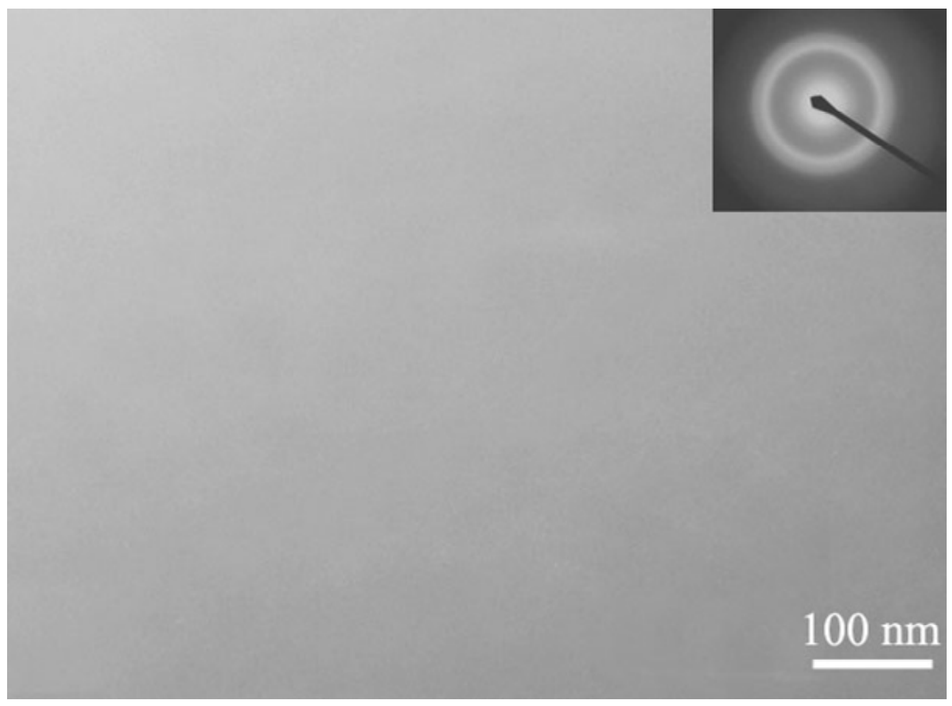

Fig. 1. TEM image of the structure of as-prepared amorphous $Ni_{70}Mo_{10}P_{20}$ alloy.

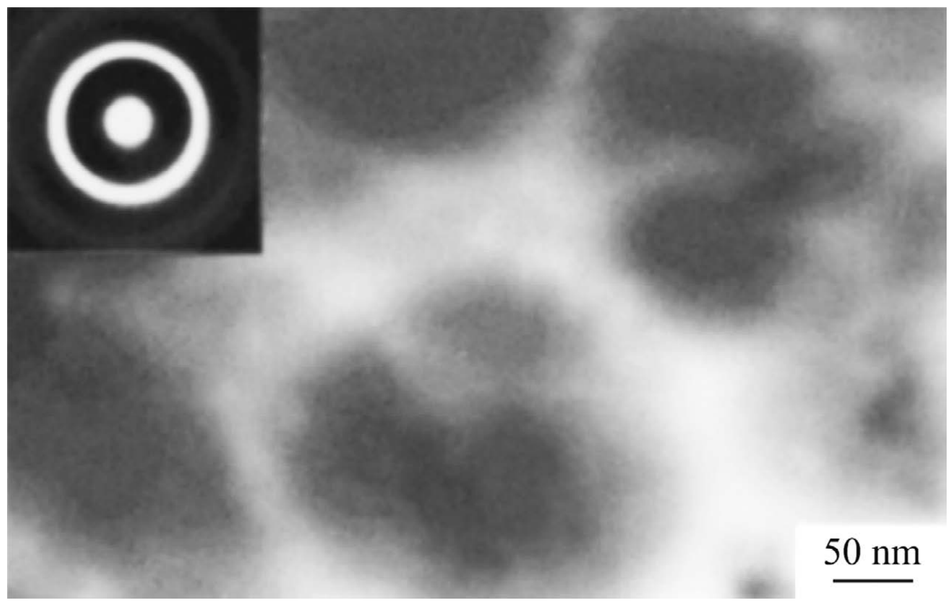

Fig. 2. TEM image of the structure of $Ni_{70}Mo_{10}P_{20}$ alloy annealed above T_g.

This leads to significant differences in the process of diffusive mass transfer in these temperature ranges, and in turn, to changes in the structure. Some examples will be discussed below.

2.1. Amorphous $Ni_{70}Mo_{10}P_{20}$ alloy

The glass transition temperature (T_g = 430 °C for heating rate of 20 °C/min) of the alloy is below the crystallization temperature (T_g = 457 °C) [37]. This allowed investigating the changes in the structure both in supercooled liquid state (above T_g) and in the amorphous state (below T_g). Heating above the glass transition temperature leads to a change of the structure of the amorphous phase. Figs. 1 and 2 show the TEM images of as-prepared sample (Fig. 1) and annealed above T_g sample (Fig. 2) [37]. Under the same conditions of preparation of electron microscopy foils, in the annealed sample, in contrast to the original, there is a pronounced spotted contrast.

The results obtained by X-ray diffraction and transmission electron microscopy methods show the appearance of the regions with different short range order and different chemical composition. With further heating, the crystallization begins in places that appear lighter in the TEM images. In these places, crystals of Ni(Mo) FCC solid solution form; the size of the crystals is 20-30 nm, and crystals are in direct contact with each other. If the heat treatment was carried out below the glass transition temperature, changes in the structure of amorphous phase were not observed. During the crystallization, as said, eutectic colonies form and the structure differs radically from that observed above the glass transition temperature.

Thus, the processes leading to separation of amorphous phase occur at the temperatures above T_g. The size of the areas with different chemical composition and/or different short-range order is about 100 nm. Crystallization of the alloy below the glass transition temperature takes place by eutectic crystallization mechanism: eutectic colonies form in amorphous matrix. In this case the redistribution of the components before the crystallization occurs insignificantly or nonexistent.

2.2. Amorphous $Ni_{70}Mo_{10}B_{20}$ alloy

In this alloy, the glass transition temperature is also below the crystallization temperature. On heating the amorphous alloy above the glass transition temperature, a width of the first diffuse peak in the X-ray diffraction patters increased [41]. This change is similar to the above change in the diffraction pattern of the amorphous $Ni_{70}Mo_{10}P_{20}$ alloy. In the alloy with phosphorus, the process of phase separation manifested in increasing the half-width of the diffuse maximum, which distorted during the annealing. This modification was due to the formation of amorphous regions with different concentrations of the components, later crystallized with the formation of different phases.

The change of X-ray diffraction pattern in $Ni_{70}Mo_{10}B_{20}$ alloy is due to the appearance of areas with different chemical compositions. Crystallization of the alloy above the glass transition temperature leads to the formation of three crystalline phases simultaneously: two face-centered crystalline phases with lattice parameters of 0.3597 nm and 0.3541 nm, and an orthorhombic phase Ni_3B type. FCC phases are Ni and Ni(Mo) solid solution. All three phases form substantially simultaneously. The crystal size is less than 50 nm. Each nanocrystal is surrounded by the amorphous matrix (Figs. 3 and 4). Studies of the structure by transmission and high resolution electron microscopy methods showed that the formation of the phases is independently from each other. It is natural to assume that the forma-

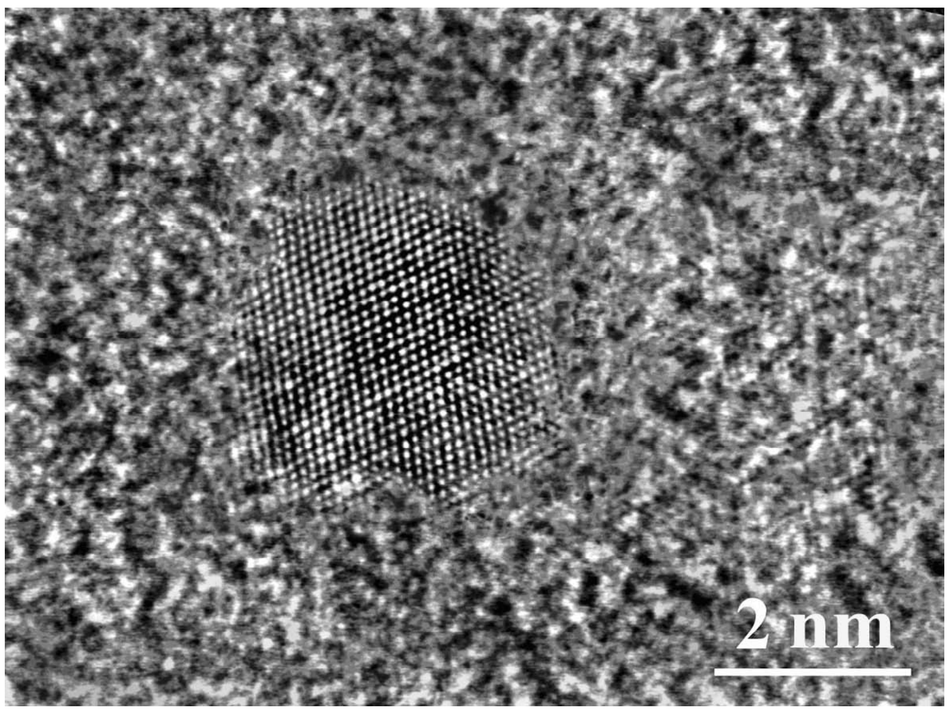

Fig. 3. HREM image of the structure of Ni nanocrystal in amorphous matrix.

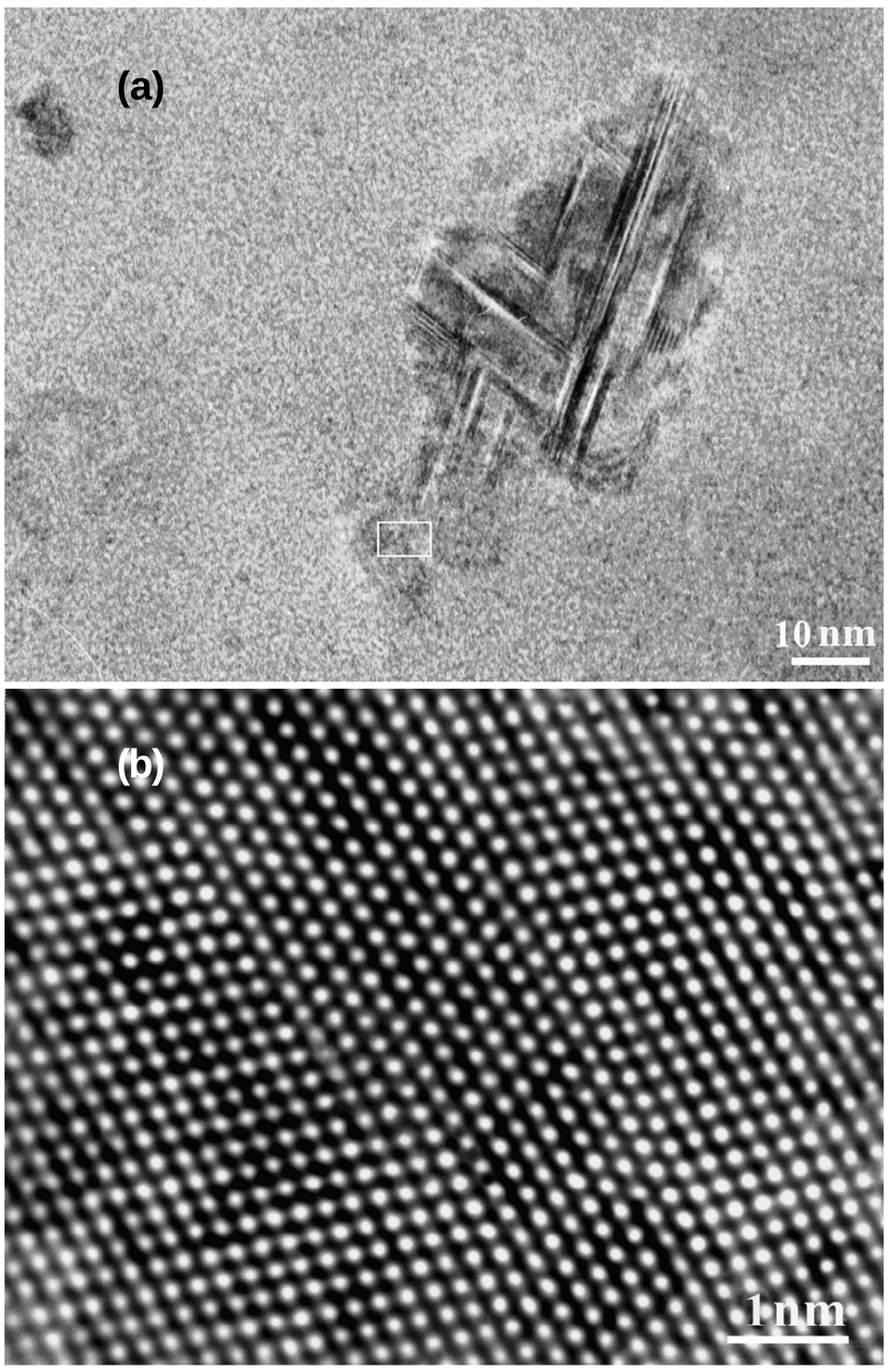

Fig. 4. HREM image of the structure of Ni(Mo) nanocrystal in amorphous matrix (*a*) and enlarged image (b) of the area circled by the frame in the figure (a).

tion of each of the crystalline phases occurs in “their” concentration region, i.e. the formation of crystalline phases in each concentration region can occur by the polymorphic mechanism without changing the chemical composition or by primary crystallization mechanism with slight change in concentration. These types of the crystallization (primary or polymorphic instead of eutectic crystallization) are due to changes amorphous structure before the crystallization which ensures the formation of amorphous regions to “fit” the compositional ordering. Below the glass transition temperature, phase separation is not observed, the crystallization occur by the eutectic mechanism.

Thus, structure formed above and below the glass transition temperature in both alloys ($Ni_{70}Mo_{10}B_{20}$ and $Ni_{70}Mo_{10}P_{20}$) are very different. It should be noted that the scale of the chemical composition change may be different: it is about some tens nanometers (15-20 nm) in (Fe-Zr system) [39] or more than 50 nm (Ni-Mo-B system) [41]. This difference is connected with opportunity of implementing a diffusion mass transport in different temperature conditions. So, above and below the glass transition temperature, amorphous structure varies differently, later leading to the formation of different crystal structure and, of course, different physical properties.

Changes in the structure of the amorphous phase do not necessarily have the character of a separation at heat treatment. The type of short-range order can vary with the temperature [42,43]. For example, depending on the temperature range order of the Fe-B amorphous phase may vary from package type of Fe_3B boride orthorhombic (Pnma space group) to tetragonal Fe_3B boride packaging type ($P4_2/n$ space group). Subsequent crystallization leads to formation of the boride with short-range order which had the amorphous phase before the crystallization.

3. NANOGLASSES

Decomposition occurring in amorphous materials is interesting in itself. The structure decomposition and changes of the chemical composition within the amorphous state are particularly important since such transformations form new amorphous phases that cannot be obtained by conventional means [44,45]. Amorphous alloys consisting of amorphous regions with different chemical composition and/or density and/or short range order named nanoglasses attracted a lot of attention due to the complex of high magnetic, mechanical, catalytic properties. Structure and properties of nanoglasses differ from both usual amorphous and nanocrystalline materials. They have a heterogeneous structure, amorphous regions with the same or different chemical composition are separated by boundaries with increased free volume Such materials are promising from the point of view of creating novel materials [46- 50].

As it was mentioned above, the coexistence of some amorphous phases was observed in a lot of systems. These phases have no sharp interfaces. Processes of amorphous phase separation may occur by different way. It was shown in [34] that separation of Pd-Au-Si amorphous phase depends on chemical composition and separation tendency increases with increasing concentration of Au. Formation of new amorphous phases in $Pd_{0.8}Au_{0.035}Si_{0.165}$ alloy takes place by nucleation and growth mechanism, later FCC phase form by primary crystallization mechanism. Amorphous $Pd_{0.74}Au_{0.08}Si_{0.18}$ alloy crystallizes after the decomposition and two crystalline phases form successive. The authors [34] have concluded that separation occurs by spinodal mechanism at least at initial stage with concentration wave of ~20 nm in length. Possibility of phase separation by spinodal mechanism was also discussed in [28]. Spinodal mechanism of amorphous phase decomposition was also considered for other metallic glasses [45,51].

Another approach is based on the use of severe plastic deformation methods to amorphous alloys. Applying severe plastic deformation leads to formation the sets of shear bands. The shear bands contain the increased concentration of free volume. They separate the areas of the amorphous matrix with the initial characteristics. When the deformation level is high, these regions contain also nanovoids. In this cased the structure is similar to nanoglass structure.

4. CHANGES OF PROPERTIES WITH AMORPHOUS STRUCTURE EVOLUTION

The physical properties of amorphous alloys are very sensitive to structure evolution; they depend on external influences. Amorphous phase is not thermally stable, so the subsequent annealing, does not leading to crystallization, causes the structure change. This is manifested in the increase of the density, Young's modulus, to embrittlement, decrease of internal friction, change of magnetic properties, etc. Naturally, the process of phase separation can lead to a significant change in the properties of amorphous alloys. For example, changes in the structure during annealing are accompanied by changes in microhardness of amorphous phase. For example, microhardness marked increases at low temperature annealing of amorphous $Fe_{80}B_{20}$ alloy [52]. Since the microhardness of the material characterizes the strength of the bonds between atoms in the structure, change of microhardness show evident amorphous structure evolution. The change of the microhardness during the annealing is obviously caused both decreasing free volume, and by ordering processes. Study of the amorphous $Fe_{27}Ni_{63}P_{14}B_6$ alloy [53] showed rising Curie temperature at heating in the temperature range below the crystallization temperature. Later, these changes were observed in a number of other alloys [54-56]. Thermocycling (heating-cooling) of the amorphous Fe-B-P alloy in the temperature range 250-350 °C was found to lead to monotonic decrease of the magnetization and a kink was observed in the dependence of derivative of magnetization with respect to temperature curve [54]; the magnitude of the kink increases with the heat treatment duration. Changing the shape of the dM/dT curve indicates the formation of regions characterized by different Curie temperatures. Thus, the heat treatment of Fe-based metallic glass can lead to separation of the amorphous phase into region differing in composition and/or short-range order, which can be characterized by different Curie temperatures.

The ductility of amorphous alloy decreases during heating. This decrease can start at a sufficiently low temperature compared to the temperature of crystallization depending on the chemical composition. The embrittlement of amorphous alloys was first detected in the $Fe_{40}Ni_{40}P_{14}B$ alloy and it was believed that it is caused by the presence of phosphorus, since it was found that the fracture surface is enriched with phosphorus [57]. However, it was shown [58] that the Fe-Si-B alloys (without phosphorus) are also fragile. The embrittlement is a distinctive feature of amorphous iron-based alloys. Study of the dependence of embrittlement showed that the phenomenon of embrittlement is peculiar to Fe alloys doped with one or two or metalloids. The embrittlement of iron-based alloys containing nonmetals of two types may be due to the separation of amorphous phase.

5. CHANGES IN THE AMORPHOUS STRUCTURE DURING DEFORMATION

The structure of amorphous phase can vary considerably, not only by heating but also at deformation. The question of a possible change in the structure under the influence of the deformation came into sight from the very beginning of amorphous alloy research. As an example, K. Pampillo reviews [59,60] should be mentioned; where problems of homogeneous deformation and inhomogeneous flow, the fracture processes, their dependence on the

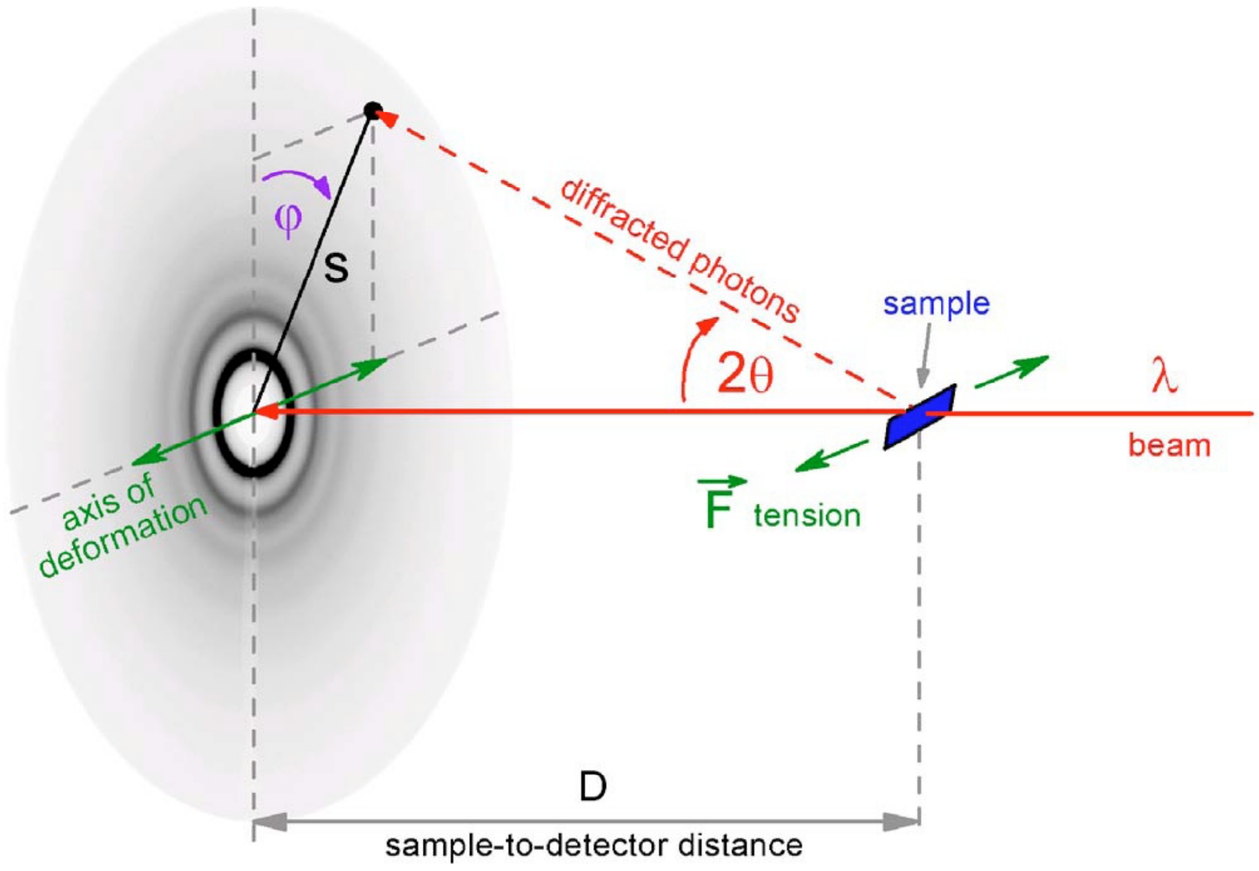

Fig. 5. Scheme of X-ray scattering measurement scheme under tensile deformation, modified from [64].

temperature and composition were discussed. Investigations of the amorphous structure under deformation were rather small.

The change in the structure of the amorphous phase at the deformation which does not lead to crystallization was studied last years. For instance, change in the structure under the influence of the hydrostatic pressure was observed in metallic glasses enriched in rare earth-rich component ($Ce_{55}Al_{45}$ metallic glass [61]). A typical feature of this transition was a significant increase in the density at the compression and hysteresis upon application – removal of the pressure. Similar phenomenon of polyamorphism was observed in other glasses (e.g., La-Ce-Al [62]). The reason polyamorphism was discussed to be due to delocalization of 4f electrons of Ce, leading to a decrease in Ce-Ce bond length. However, such a phenomenon is not observed at all metallic glasses that are rich in the rare earth component (e.g., $La_{75}Al_{25}$).

Some researches on the structure evolution carried out directly in the process of deformation of Zr-based amorphous alloys aroused great interest. The samples were deformed by tension and synchrotron source was used for structure investigations in-situ. It allowed detecting the structure occurring at the elastic deformation [63-65]. Fig. 5 [64] shows a scheme of in-situ X-ray measurements of amorphous $Zr_{64.13}Cu_{15.75}Ni_{10.12}Al_{10}$ alloy subjected to tension.

The experiments were carried out in transmission geometry, the load varied with increments of 400 °C. It has been found that in the absence of plastic deformation, the tensile results in a change of the distance between atoms in an amorphous

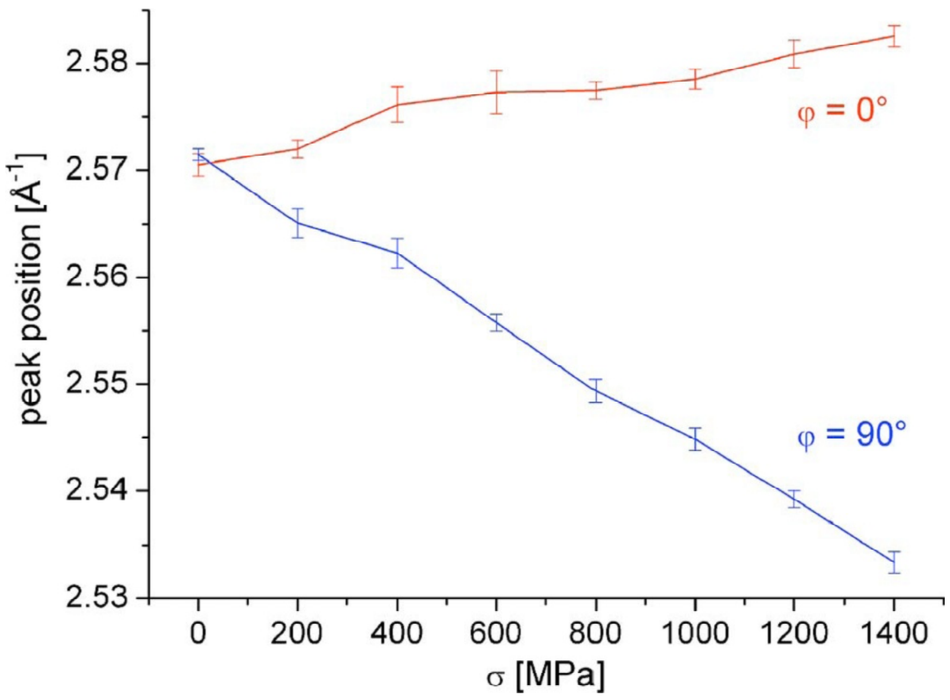

Fig. 6. The dependence of the first diffuse peak position the X-ray diffraction pattern one applied stress (φ = 90 - in the direction of the applied stress, φ = 0 - in the transverse direction).

structure, and these changes depend on the orientation of the applied stress. Fig. 6 shows the change in position of the first diffuse maximum depending on the applied stress σ. It is evident that the initial symmetric with respect to zero diffuse peak position becomes asymmetric in the process of deformation. The results indicate that the first coordination sphere, characterizing the arrangement of atoms in the amorphous structure transformed into an ellipsoid in the deformation process.

In the study of elastic deformation of $Zr_{62}Al_8$, $Ni_{13}Cu_{17}$ and $La_{62}Al_{14}(Cu_{5/6}Ag_{1/6})_{14}Ce_5Ni_5$ metallic glasses the deformation was shown [63] to be indeed an anisotropic (Fig. 7). For comparison, the figure also shows the “stress-strain” curves for bulk metallic glasses of the same composition (black lines). For details changing the top of the first diffuse maximum for Zr_{62} Al_8 $Ni_{13}Cu_{17}$ metallic glass during deformation is shown in Fig. 8 [63].

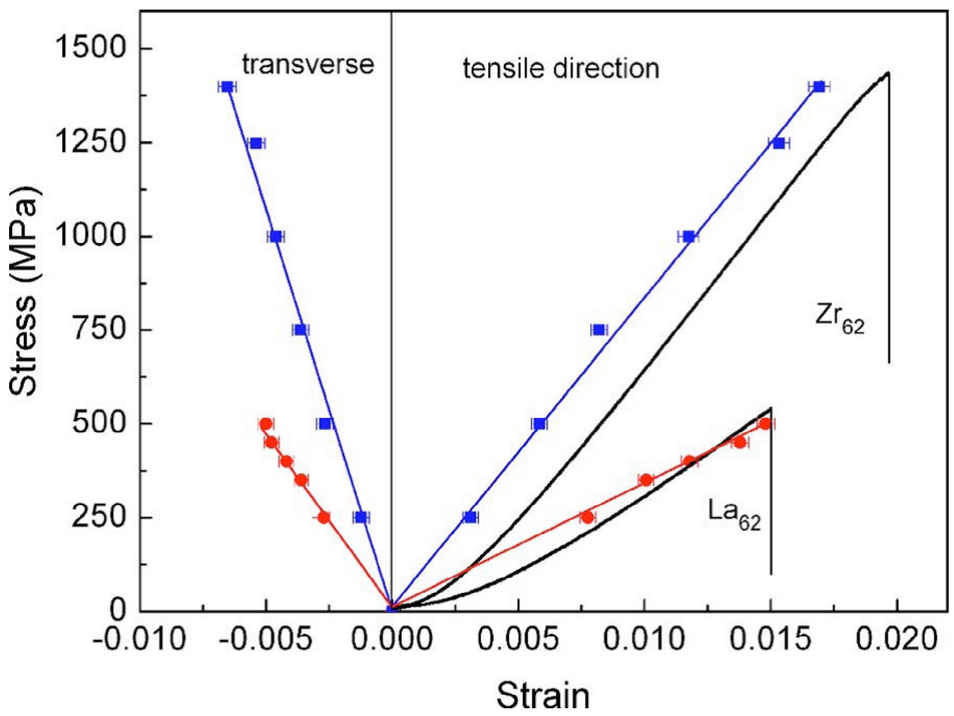

Fig. 7. Stress-strain dependence in the direction of the applied stress and in the transverse direction (color lines), modified from [63]. Circles and squares correspond to La_{62} and Zr_{62}, respectively.

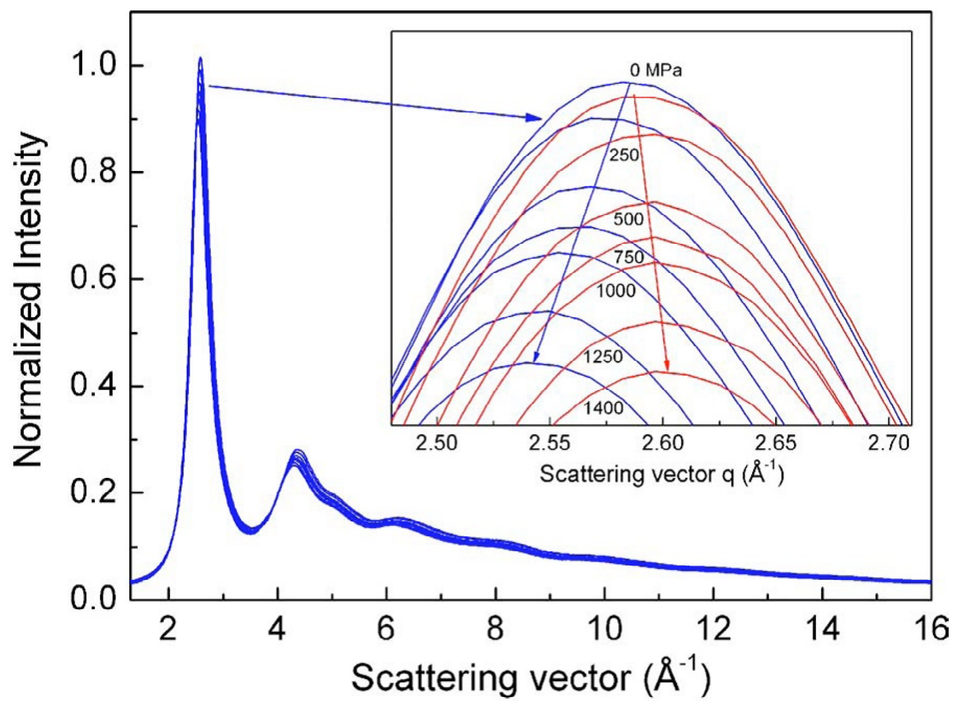

Fig. 8. Change of the top of the first diffuse maximum for $Zr_{62}Al_8Ni_{13}Cu_{17}$ metallic glass during deformation, modified from [63].

Thus, in the absence of plastic deformation, tensile may result in a change of the distance between atoms in an amorphous structure, and these changes depend on the orientation of the applied stress. The Zr-based amorphous alloys are brittle and they practically do not undergo plastic deformation, so only the region of elastic deformation was considered in above paper. At the same time it would be interesting to determine whether the observed changes in the structure can be stored when the load is removed and whether they exist at plastic deformation. Such studies have been carried out for the amorphous $Pd_{40}Ni_{40}P_{20}$ alloy. The samples were subjected to multiply rolling deformation and the structure was studied along and across the rolling direction [66]. It was found that amorphous sample structure becomes anisotropic after deformation. It can be seen (Fig. 9) that the diffuse maxima of the sample obtained for different mutual orientation of the X-ray beam and the sample are displaced relative to each other. The shortest distances between atoms were identified from these X-ray diffraction patterns. The distance between atoms along the rolling direction was found to increase at the deformation, whereas it does not change in the perpendicular direction. The observed effect reduced over time.

The results obtained for amorphous $Pd_{40}Ni_{40}P_{20}$ alloy revealed: the difference (anisotropy) in the X-ray scattering by the deformed samples along and across the direction of deformation manifesting itself in the different position of the diffuse maxima

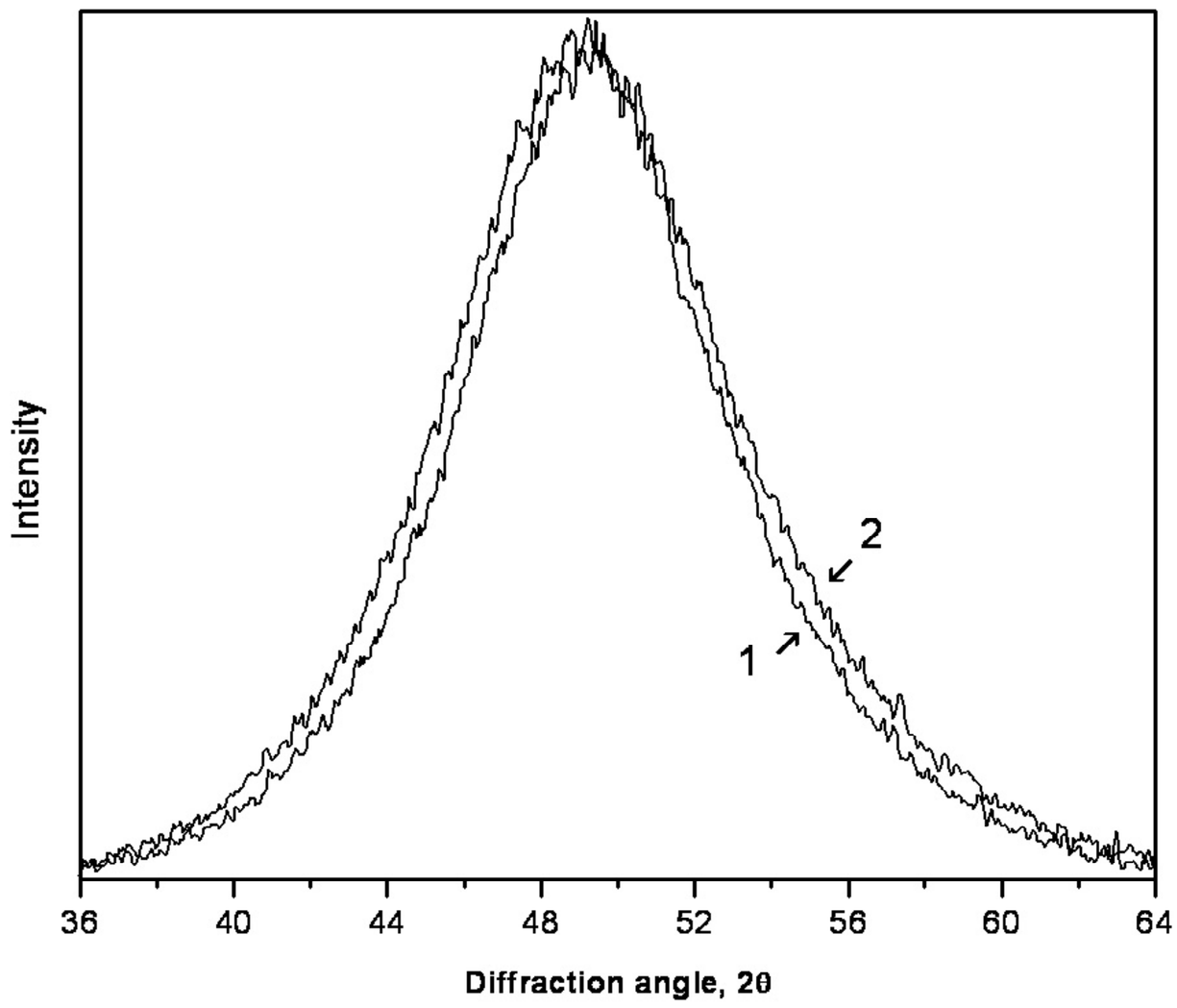

Fig. 9. An initial part X-ray diffraction pattern of the sample after rolling.

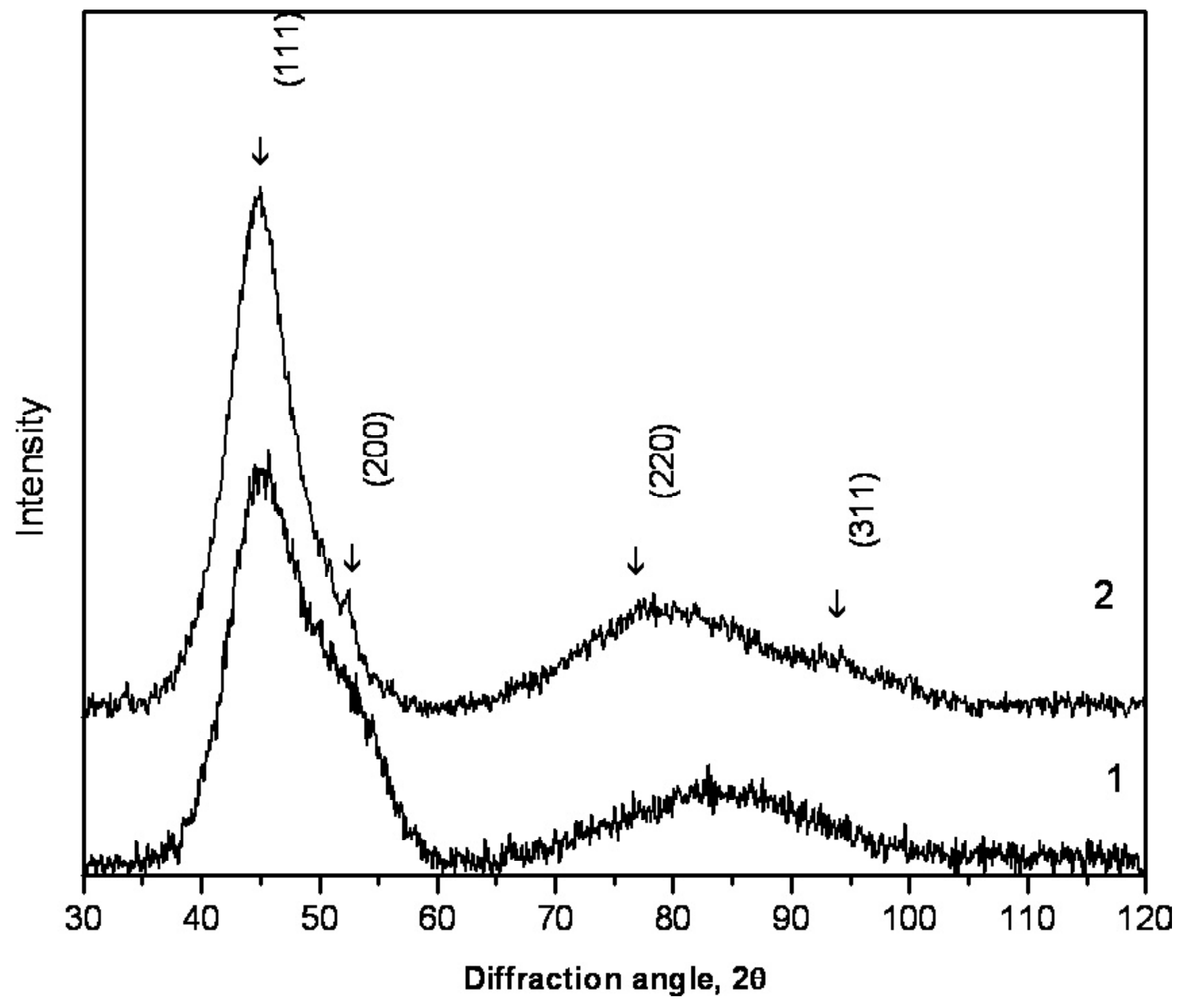

Fig. 10. X-ray diffraction patterns of deformed $Al_{88}Ni_{10}Y_2$ (1) and $Al_{88}Ni_2Y_{10}$ (2) alloys.

on the X-ray diffraction pattern obtained by X-ray diffraction analysis of the sample along and across the direction of rolling; and attenuation of the observed effects (scattering anisotropy and changes of the velocity of sound) in the course of time. The shortest interatomic distances were calculated and it was shown that the rolling causes the changes of the amorphous phase structure (distortion of the first coordination sphere). The structural changes are more pronounced in the surface.

Thus, the deformation process changes the structure of the amorphous phase. Since plastic deformation of amorphous alloys is achieved by formation and propagation of shear bands, feasible structural changes were analyzed both in the shear bands and in the shear band-free areas of the amorphous phase. The observed effect is shown to be induced by inelastic deformation of the amorphous phase chiefly in the shear band-free areas. The effects diminish with aging of the deformed samples which confirms the hypothesis about inelastic deformation of the amorphous phase.

As noted above, the effect of the elastic deformation on the structure of metallic glasses was studied in a group of Zr-based amorphous alloys [63-65]. The results clearly showed an elliptical character of the first coordination “sphere”. In the case of the $Pd_{40}Ni_{40}P_{20}$alloy, the samples were deformed inelastically, and plastically, and the anisotropy of the structure remained after the removal of the plastic deformation, so the causes of changes in the distances between the atoms can be more complex.

In accordance with Hooke’s law, elastic deformation during elongation is linearly dependent on the stress. At higher loads, this dependence deviates from the linear law, which is due to inelastic deformation whose magnitude in amorphous alloys is about an order of magnitude more than that in crystalline alloys. This inelasticity is associated with the free volume in the amorphous structure: if the free space is small, inelastic deformation is also small. Inelastic deformation decreases after annealing at which the structural relaxation occurs. At high stresses and relatively low temperatures, deformation occurs heterogeneously and it is much localized. Narrow shear bands formed, the orientation of the shear bands is close to the orientation of the maximum shear stress. Another characteristic feature of plastic deformation of amorphous alloys is increasing concentration of free volume in the shear bands, i.e., increasing average interatomic distance. Since shear bands are distinguished by disordered structure of the amorphous phase and low density regions in which the mean interatomic distance is somewhat larger than in the basic amorphous matrix, the structure of the deformed samples can be regarded as “double-phase”, the first “phase” being the original amorphous alloy and the other “phase” the material in the shear bands. Then the diffuse peaks in the X-ray diffraction patterns make up a superposition of two diffusion maxima from each “phase”. It should be remembered, however, that the share of the material in the shear bands is not large and, hence, its contribution to scattering will be

negligible. Hence, as in the case of heat treatment, the observed change in the shape of the diffuse maximum revealed by the X-ray diffraction patterns is conditioned by formation of regions with a type of short-range order and composition different from those of the matrix. Naturally, this does not exclude a different structure of the material in shear bands, but, owing to the negligible contribution to scattering, its share can hardly be estimated.

In addition to occurrence of the anisotropy in the structure, plastic deformation may lead to separation of the amorphous phase.

Heat-induced decomposition of the amorphous phase was also observed in the amorphous Al-Ni-Y system alloys. The alloy samples were subjected to plastic deformation by way of multiple rolling [67]. Note that changing the structure under the influence of plastic deformation depends on the alloy composition. Fig. 10 shows the X-ray diffraction patterns of amorphous $Al_{88}Ni_2Y_{10}$ and $Al_{88}Ni_{10}Y_2$ alloys after deformation by multiply rolling. It is evident that the first diffuse maximum from the $Al_{88}Ni_{10}Y_2$ sample (curve 1 in the X-ray diffraction pattern) is asymmetric and, obviously, it is a superposition of at least two maxima. Two amorphous halos indicate the appearance of regions, which differ in composition. Based on analysis of the atom size and compositions of the metallic glasses one may easy conclude that the two diffuse maxima correspond to the regions, enriched and depleted by yttrium (and/or nickel). Thus, rolling of the $Al_{88}Ni_{10}Y_2$ alloy leads to separation of the amorphous phase into regions with different chemical compositions.

In X-ray diffraction pattern of the $Al_{88}Ni_2Y_{10}$ alloy (curve 2, Fig. 10) weak reflections (marked by arrows in the figure) corresponding to Al nanocrystals appeared after the deformation. The first peak in the X-ray diffraction pattern is a superposition of an amorphous halo and the (111) Al Bragg reflection. The intensity of the reflections from the crystalline phase is very weak due to a small amount of crystals of Al, dispersed in an amorphous matrix.

Thus, deformation at room temperature leads to the formation of crystals in the amorphous matrix. After increasing the deformation level at room temperature, the $Al_{88}Ni_2Y_{10}$ structure does not appreciably change, and a small amount of Al crystals also appears in $Al_{88}Ni_{10}Y_2$ metallic glass. Consequently, the deformation of metallic glasses can lead both to separation of the amorphous phase, and development processes nanocrystallization even at room temperature.

Deformation of amorphous phase also leads to change of different properties of the material [68].

6. NANOCRYSTAL FORMATION AT HEAT TREATMENT AND DEFORMATION

As it was mentioned above, formation of nanocrystals at heat treatment can occur by different crystallization mechanism depending on chemical composition and prehistory of the samples. In most cases the crystallization of the amorphous phase occurs by the mechanism of nucleation and growth. The transition of the amorphous phase into crystalline phases depending upon the alloy composition can occur by one of the following reactions:

- primary (or preferential) crystallization: the formation of the crystals with chemical composition different from the composition of initial amorphous phase;
- eutectic crystallization: the simultaneous formation of two crystalline phases and
- polymorphic crystallization: crystallization occurs without changing the chemical composition.

Nanocrystalline structure usually forms by primary crystallization mechanism. Nanocrystalline materials may be single-phase and multiphase polycrystalline samples with a grain size up to 100 nm (at least in one direction). Due to the extremely small size of the grain the structure of nanocrystalline materials is characterized by a large volume fraction of grain boundaries and interfaces, which can largely determine a variety of physical and chemical properties of the material. Indeed, it has been found that many properties of nanocrystalline material are fundamentally different from those of conventional polycrystalline and amorphous alloys [69,70]. For instance, nanocrystalline materials may have high strength and hardness, good ductility and toughness, reduced elastic modules, higher diffusion rates, large heat capacity and thermal expansion coefficient, and higher magnetic properties as compared to conventional materials.

The main advantage of the method of nanostructure formation by controlled crystallization of amorphous alloys is the ability to control the process kinetics by optimizing the heat treatment parameters (temperature and annealing time) and the simplicity of the method. In the most amorphous alloys, nanocrystallization can be carried out in conventional annealing, that provides a large amount of nanocrystalline samples. Moreover, by changing the heat treatment conditions, it is possible to obtain samples with different grain sizes ranging from a few nanometers to microns [71].

However, the amorphous phase can crystallize with nanostructure formation only in some alloys. A

new method for producing nanostructures has been recently developed: nanocrystallization of amorphous alloys subjected to deformation [72]. In both cases, thermal treatment and deformation, the process of nanocrystal formation is determined by the higher parameters of diffusion mass transfer.

Applying different types of deformation to amorphous materials makes it possible to obtain nanocrystalline alloys with new compositions (including alloys, which can not be obtained in the nanocrystalline state by conventional methods), as well as allows obtaining nanocrystalline samples of larger size. Currently, there are a number of research in which the authors compared the parameters of nanostructures formed during heat treatment and deformation [13-15,17,18,67].

Severe plastic deformation of amorphous alloys leads to the formation of nanocrystals, and the nanocrystals location correlates with the location of shear bands [22]. One of the existing today explanations of such localization of the nanocrystals is the assumption that the plastic deformation leads to increasing temperature in the shear bands up to the melting temperature [73]. According to the calculations, the temperature in the shear bands can reach up to 1000 °C and persists for a few nanoseconds. If this local increase in temperature is higher than the crystallization temperature of the amorphous phase and this increase lasts enough long, the crystallization of the amorphous phase can occur by diffusive nucleation and growth mechanism. The second approach to explain the correlation of the nanocrystals and shear bands location is based on the difference in the structure of the amorphous phase in shear bands, and in places free of shear bands. The structure of the shear bands are more disordered, the share of free volume is higher, the processes mass transfer and, hence, the crystallization is facilitated in these areas. The nanocrystal formation is spatially associated with places of localization of plastic deformation (shear bands). As to spreading of individual shear bands, the propagation velocity in the bulk amorphous is known to be irregular; there is a so-called «stick-slip» dynamics typical for granular structure [74]. Such dynamics should be thermally activated, depending on the kinetics of the free volume supply to the shear bands and free volume relaxation. In this connection, the use of severe plastic deformation to amorphous alloys looks very attractive. This processing method allow to vary widely the level and conditions of plastic deformation; and therefore the quantity, the location and the parameters of shear bands and, hence, the forming nanocrystals.

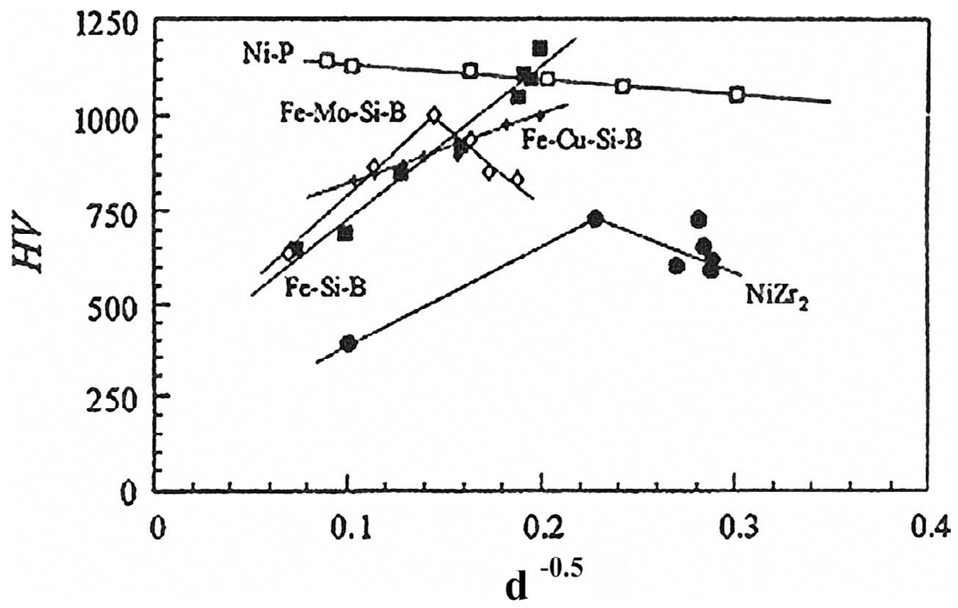

Fig. 11. Dependence of microhardness on nanocrystal size.

7. MECHANICAL PROPERTIES OF NANOCRYSTALLINE ALLOYS

One of the most important changes that occur in polycrystalline materials with decreasing grain size is increasing strength and hardness. As is known for conventional polycrystalline metals, the yield strength σ_y is inversely proportional to the square root of grain diameter *d* [75, 76]:

$$\sigma_t = \sigma_0 + K_y / d^{1/2}, H_v = H_{v0} + K_h / d^{1/2},$$

where σ_y is yield strength, σ_0- lattice friction stress that occurs when moving a single dislocation and it does not depend on the grain size, K_t - constant (positive), depending on the resistance of the grain boundaries to the motion of dislocations, H_v - microhardness, and $\sigma_t \approx H_v/3$.

Nanocrystalline materials with an extremely small grain size are of great interest in this context. Studies of the mechanical properties of nanocrystalline materials have shown that the noted dependence is often violated when the size of the crystals becomes less than 50 nm. The performing or omitting the Petch-Hall law depends on the method of the material producing. Fig. 11 illustrates the different behavior in microhardness depending on the grain size for alloys produced by controlled crystallization of metallic glasses [77]. In these materials, there is a critical size of the grain [77,78]. If grain size is more than critical size, the law Petch-Hall is satisfied, otherwise deviations from it, or even an inverse relationship is observed. As mentioned earlier, critical grain size was observed in nanocrystalline materials, from which the Petch - Hall dependence becomes inverse ratio (Fig. 11). After first stage of crystallization an anomalous behavior of the Petch-Hall relation is usually observed: strength of the nanocrystalline alloys grows with increasing grain size (i.e., the proportion of the crystalline phase).

The strength characteristics of the alloy are maximal for critical size of the nanocrystals. The kink in the dependence of the tensile strength on the nanocrystal size involves changing the deformation mechanism from dislocation mechanism (in the case of the Petch-Hall law) to the other, for example (but not necessarily), grain boundary sliding. The implementation of this or that mechanism depends on the structure of the material.

Obviously, as mentioned above, the direct application of the Petch-Hall ratio to the materials considered in this study is impossible. Firstly, Petch-Hall equation is applicable for hardening, caused by accumulation of dislocations on the physical barrier, such as grain boundaries. Secondly, the material should be crystalline, however the nanocrystalline structure is two-phase one (amorphous - crystalline); it consists of the nanocrystals distributed in the amorphous matrix and the nanocrystals size commensurate with the thickness of the layer of the amorphous phase between the nanocrystals. There are other limitations. However, the analogy between the change in the nanocrystal size and hardening is often considered in accordance with the Petch - Hall equation.

Deformation of amorphous alloy occurs by the formation and propagation of the shear bands. In the amorphous-nanocrystalline materials, the spreading shear bands interact with the nanocrystals. The interaction of shear bands and nanocrystals play a major role in the mechanical properties of nanocrystalline materials. The different types of interactions that lead to the different mechanical properties are describes in detail in [79,80]. As it was shown in [81], the mechanism of the interaction may be different on the sizes both the nanocrystals and shear bands. The shear bands shear bands can “cut” nanocrystals, shut down, absorb them, they may ignore the nanocrystals. Mechanical properties of the material depend on this interaction. The optimum combination of high strength and ductility of Al-TM-RE alloys was found to achieve for certain sizes of nanocrystals of Al and their volume fraction [82,83]. In a conventional nanocrystallization of the amorphous alloys by heating, the size of the nanocrystals in the final step usually depends only on the chemical composition. Application of the deformation to the amorphous alloys allows formation of nanostructure with other parameters. This makes it possible to create a structure with nanocrystals of different sizes. It should also be noted that, since the plastic deformation when administered in a large amount

From the viewpoint of the mechanical properties, particular interest is connected with light nanocrystalline alloys (Mg- or Al-based alloys). These materials exhibit high strength with good ductility. At the transformation from amorphous to nanocrystalline state, the strength of the Al-TM-RE alloys containing 80-90 at.% Al significantly increases. The strength can reach values of 1.6 GPa when the specific weight is about 3.3 g cm^{-3} [6] at room temperature and 1 GPa at 573K, which is 3 and 20 times higher than the corresponding values for commercial high-strength aluminum alloys [84].

8. NANOSTRUCTURE FORMATION IN SOME AL-BASED ALLOYS FORMED AT HEAT TREATMENT AND DEFORMATION

As it was discussed, mechanical properties depend strongly on the structure. In order to produce materials with the desired combination of properties, it is necessary to form the desired structure, which, in turn, requires knowledge of the processes that determine the formation of a structure. In connection with the above, a comparative study of nanocrystal formation in amorphous alloys under heating and deformation may be interest. Binary and ternary aluminum-based amorphous alloys were chosen as research objects in which nanocrystalline structure can be formed by deformation and thermal treatment. Formation of nanostructure at heat treatment and deformation was studied in a group of Al-based alloys. Amorphous $Al_{90}Y_{10}$, $Al_{87}Ni_8La_{5,}$ $Al_{87}Ni_8Gd_5$, $Al_{87}Ni_8Y_5$, $Al_{88}Ni_2Y_{10}$, $Al_{88}Ni_{10}Y_2$, and $Al_{85}Ni_6Co_2Gd_6Si_1$ alloys were obtained as ribbons by rapid melt quenching. The samples were subjected to isothermal annealing and heating with a constant rate in a differential scanning calorimeter as well as to plastic deformation that was performed at room temperature by multiple rolling and high pressure torsion (4 GPa) in Bridgman anvils.

The structure of the sample was studied by the methods of X-ray diffraction, transmission, scanning and high resolution electron microscopy. X-ray diffraction analysis was made using a SIEMENS D-500 diffractometer with Co K_α radiation. The spectra obtained were processed with the use of special programs that allowed smoothing, background correction, separation of overlapping maxima, etc. The samples for electron microscopy studies were prepared by ion milling. For structural investigation by transmission electron microscopy method, the foils were prepared from the middle of the radius of HPT

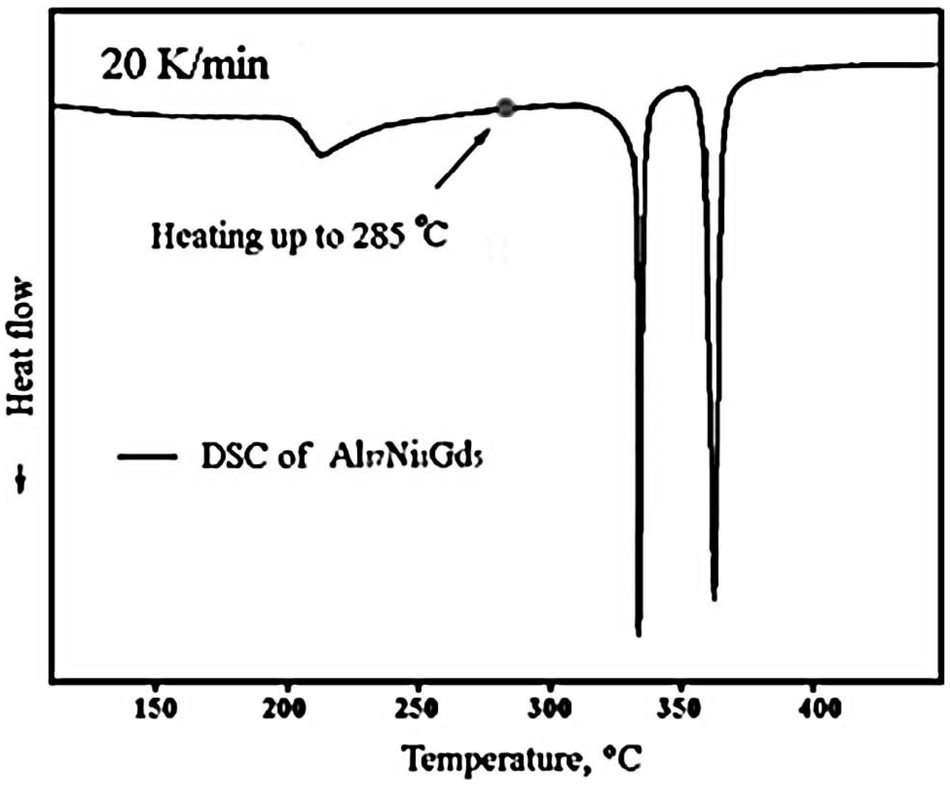

Fig. 12. DSC curve of $Al_{87}Ni_8Gd_5$ alloy.

deformed samples. The diameter of the samples for HPT was 8 mm.

All the prepared samples were amorphous. On heating crystallization of all the alloys started with formation of aluminum nanocrystals. All the samples to be compared were heated to the temperatures of a beginning, top and end of the first peak on the DSC curves corresponding to the first crystallization stage. Fig. 12 shows the DSC curve of the $Al_{87}Ni_8Gd_5$ alloy sample obtained on heating at a rate of 20 K/min to 450 °C. It is seen that crystallization of the amorphous alloy proceeds in three stages, the first resulting in precipitation of aluminum nanocrystals.

Fig. 13 presents the X-ray diffraction pattern of the $Al_{87}Ni_8Gd_5$ alloy sample after heating to the temperature of 285 °C corresponding to the end of the first crystallization stage (Fig. 12). On heating the samples contain an amorphous phase and aluminum nanocrystals. The nanocrystal size was determined by diffractometry data as well as dark field electron microscopy images. The nanocrystal size was estimated by the halfwidth of the diffraction line using the known Selyakov-Sherrer formula [85]. The fraction of the nanocrystalline phase was estimated by the ratio of the integral intensities of the reflections in the X-ray diffraction patterns [86].

As soon as the $Al_{87}Ni_8Gd_5$ sample is heated to 285 °C corresponding to the end of the first crystallization stage, the average nanocrystal size is 26 nm, the nanocrystal fraction being approximately 23%.

Fig. 14a shows the microstructure of the sample after severe plastic deformation achieved by high pressure torsion (4 GPa, 5 rotations) and Fig. 14b presents the high resolution electron microscopy image of the same sample. After severe plastic deformation the average nanocrystal size does not exceed 6 nm, the nanocrystal fraction making up approximately 25%.

For comparison Fig. 15 presents the X-ray diffraction patterns of the samples obtained as a result of heating to 285 °C and severe plastic deformation. It is seen that the widths of the X-ray diffraction lines are significantly different, which is indicative of different nanocrystal sizes. The size of the nanocrystals formed by severe plastic deformation is appreciably smaller than that of the nanocrystals produced on heating. The investigation of the fine aluminum nanocrystal structure using high resolution electron microscopy revealed that the nanocrystals did not contain any linear defects (dislocations). It should be noted that the

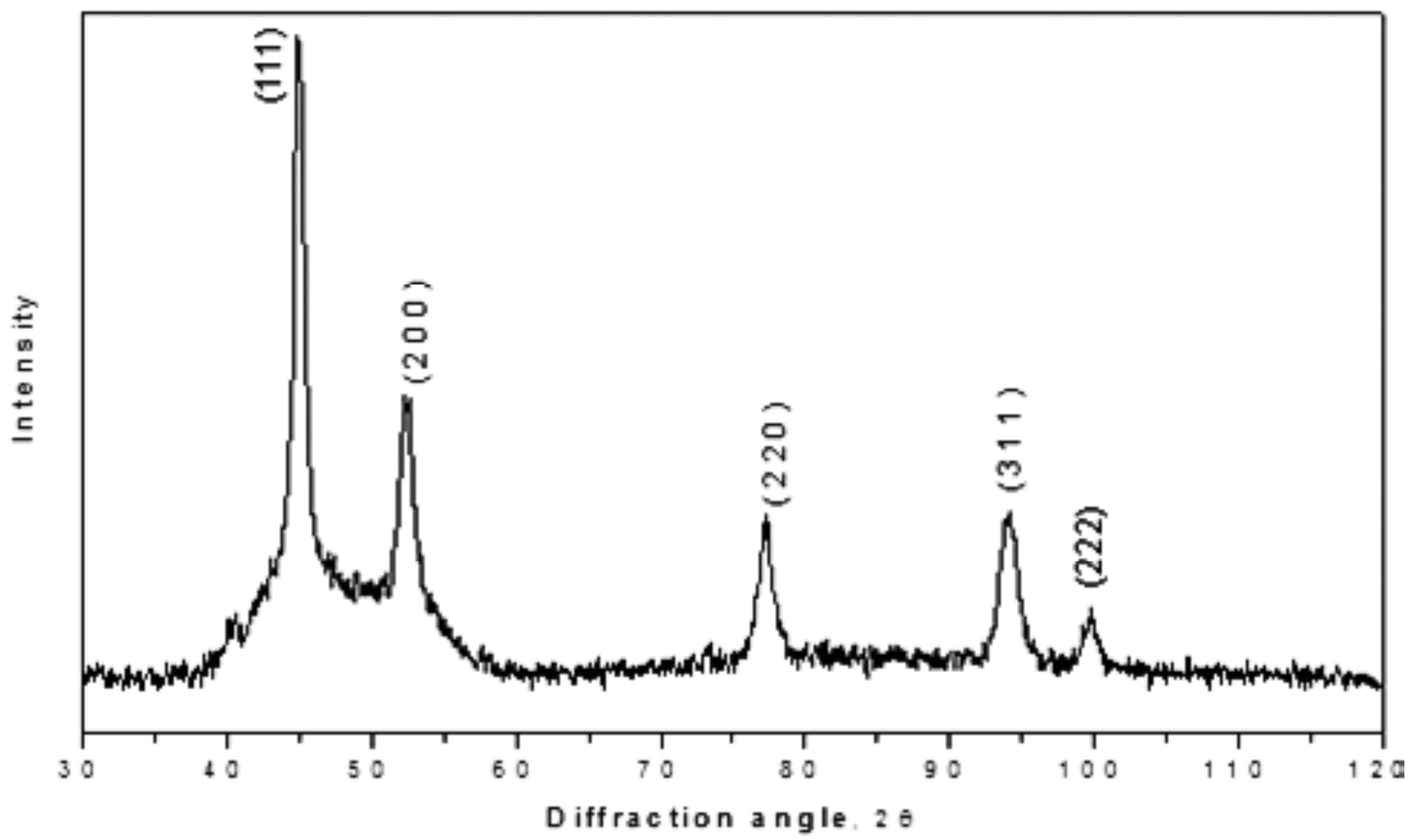

Fig. 13. X-ray diffraction pattern of $Al_{87}Ni_8Gd_5$ alloy on termination of the first crystallization stage.

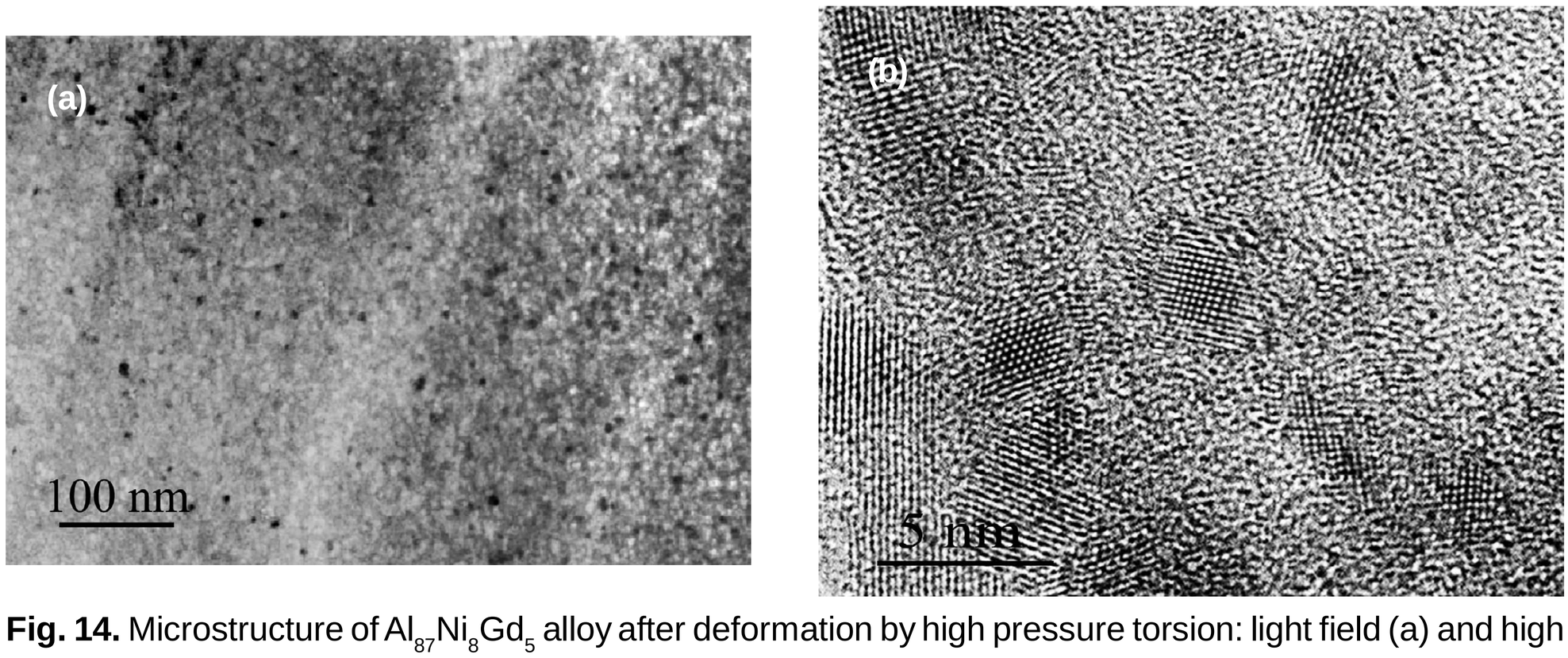

Fig. 14. Microstructure of $Al_{87}Ni_8Gd_5$ alloy after deformation by high pressure torsion: light field (a) and high resolution (b) electron microscopy images.

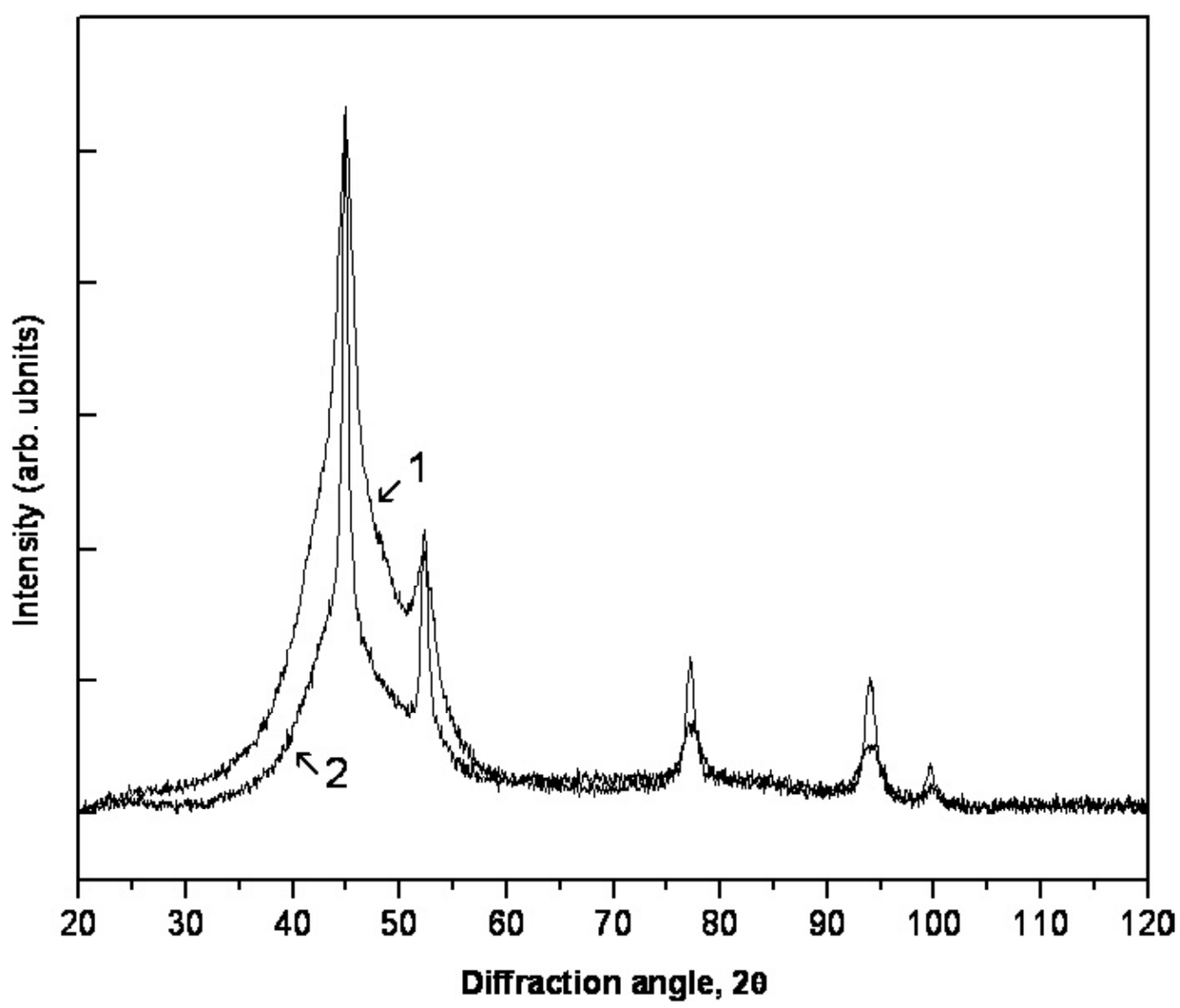

Fig. 15. X-ray diffraction patterns of samples after heating to 285 °C and severe plastic deformation.

nanocrystals formed on heating contained no dislocations as well [87]. According to [88], the dislocation-free structure of the aluminum nanocrystals is well described by their small size and chemical composition (absence of appreciable dissolution of other alloy components in the aluminum nanocrystals).

It is notable that in the deformed (SPD) samples the nanocrystals are, at first sight, arranged homogeneously and unrelated to the shear bands. It is known that at low temperature (room and lower), plastic deformation of amorphous alloys proceeds by way of formation and propagation of shear bands. The shear bands form steps on the sample surface. Fig. 16 shows surface images of deformed amorphous $Al_{87}Ni_8Gd_5$ alloy samples exhibiting network of numerous steps. The spacing between the shear bands can be several tenths of a micron (see Fig. 16). Authors of [89] present hardness profiles (measured by nanoindentation) across a single shear band in a Zr-based BMG deformed in uniaxial compression to plastic strains of 2%, 4%, and 6%. The size of the region with characteristics different from those of the matrix is about 150 nm across the shear zone. Therefore, it may be assumed that following HPT or multiple rolling, when the shear band spacing is only several tenths of a micron, the main part of the matrix displays characteristics that are different from the initial (prior to deformation), which enables easy nucleation of nanocrystals in the matrix.

It would be reasonable to assume that the use of combined treatment will allow specified variations of nanocrystal sizes. Fig. 17 demonstrates the

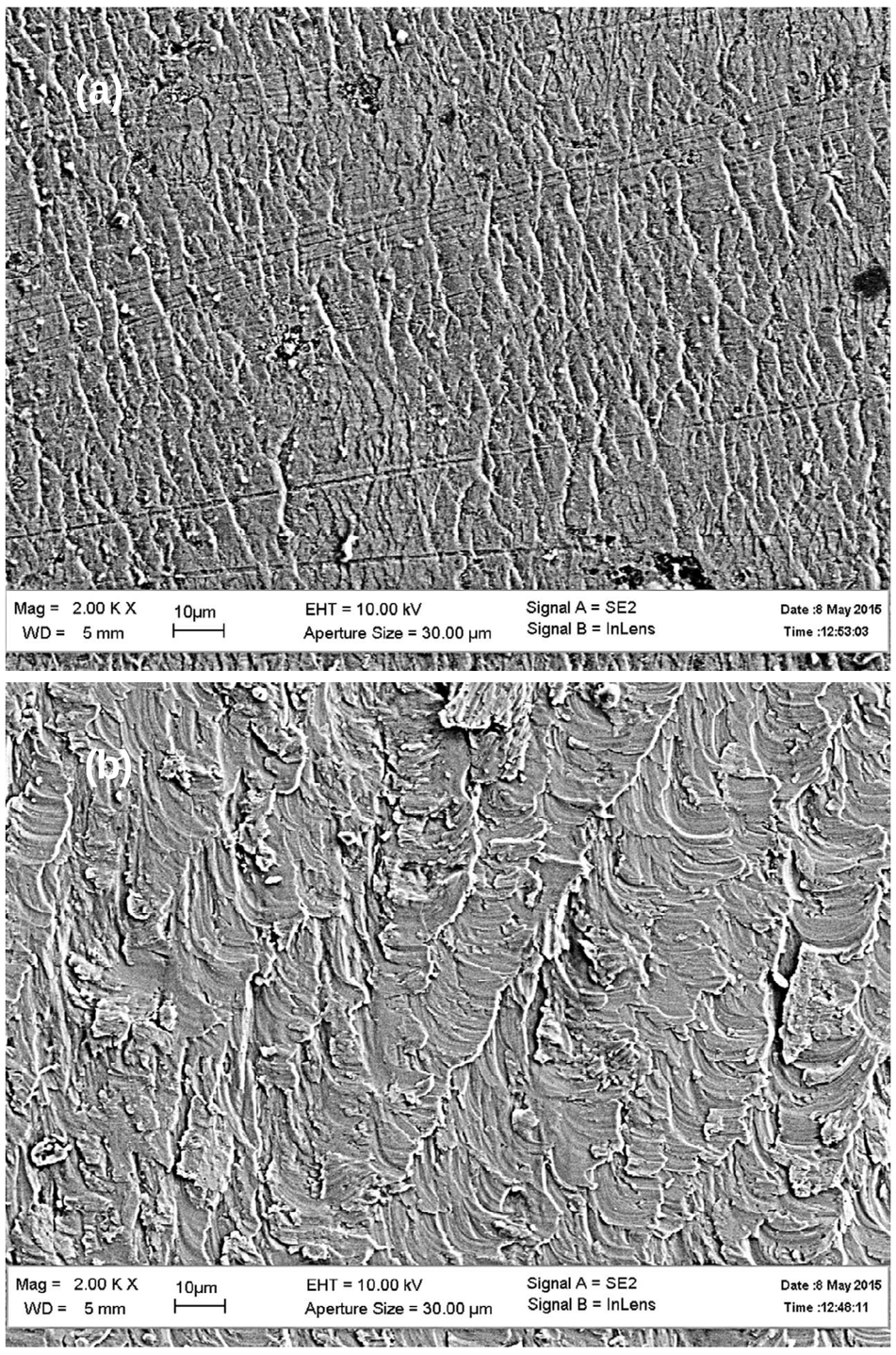

Fig. 16. Surface images of amorphous $Al_{87}Ni_8Gd_5$ alloy samples after cold-rolling (a) and HPT (b).

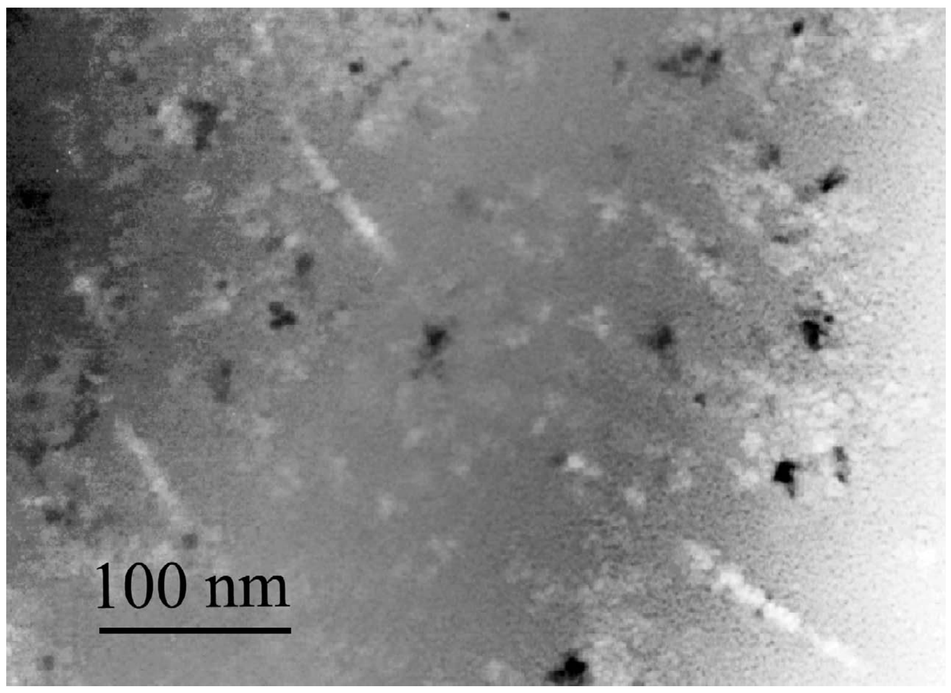

Fig. 17. Microstructure of $Al_{87}Ni_8Gd_5$, alloy after deformation and subsequent annealing.

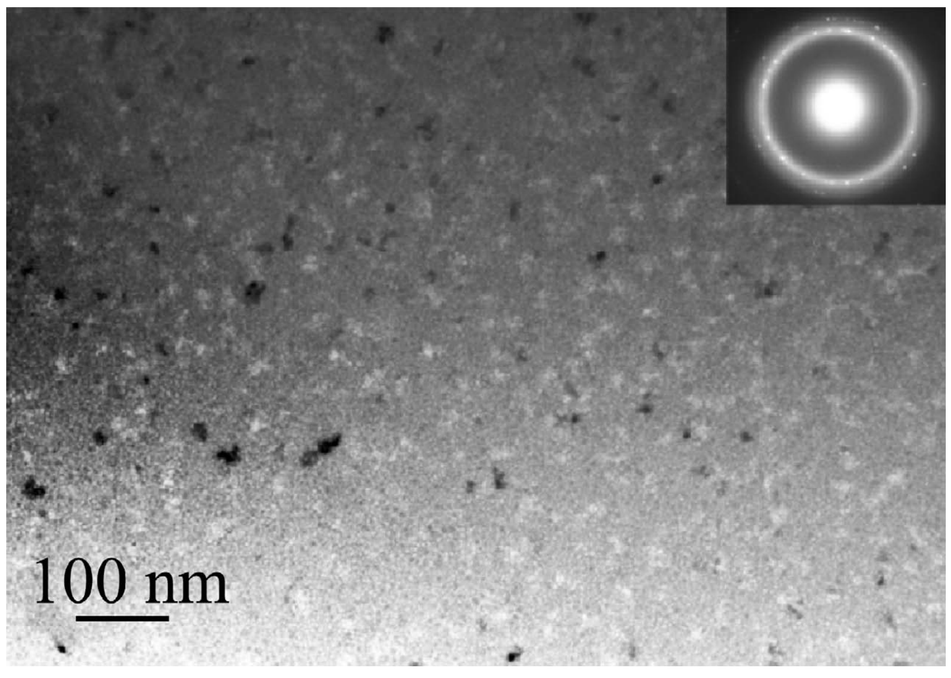

Fig. 18. Microstructure of annealed $Al_{87}Ni_8Gd_5$ alloy.

microstructure of the $Al_{87}Ni_8Gd_5$ alloy sample subjected to isothermal annealing at 175 °C for 1 after multiply rolling. The images show clear deformation bands and nanocrystals, their average size being 9 nm. If the sample was not pre-deformed, but subjected only to thermal treatment, the average size of the nanocrystals was 14 nm (Fig. 18).

Thus, the size of nanocrystals forming in amorphous alloy is essentially dependent on treatment conditions: it is minimal (6 nm) after high pressure torsion, maximal (26 nm) after heating to the temperature of the end of the first crystallization stage and intermediate (9 nm) on combined treatment (deformation + annealing). Fig. 19 shows comparative nanocrystal size distributions for the annealed, both as-prepared and pre-deformed samples which provide a clear illustration of formation of small size nanocrystals in the case when thermal treatment is preceded by plastic deformation.

Similar results were obtained in the studies of other alloys of this same group. Table 1 summarizes up the values of nanocrystal sizes and nanocrystalline phase fractions in alloys after different types of treatment.

All the investigated systems exhibited some common features:

- the sizes of the nanocrystals forming during plastic deformation are smaller than those of the nanocrystals forming on thermal treatment;
- the sizes of the nanocrystals do not change (Al-Ni-Gd, Al-Y) or change only slightly (Al-Ni-La), with increasing degree of plastic deformation whilst their volume content increases;
- the fraction of nanocrystals in the deformed samples is somewhat larger than that in the samples subjected to thermal treatment;
- combined treatment (plastic deformation + annealing) results in intermediate sizes of nanocrystals.

Thus, the formation of nanostructures with definite characteristics depends on many parameters:

- chemical composition of the alloy;
- changes occurring within the amorphous state before the beginning of crystallization (amorphous phase separation and the formation of several amorphous phases; structural changes in shear bands and in the vicinity surroundings during the deformation);

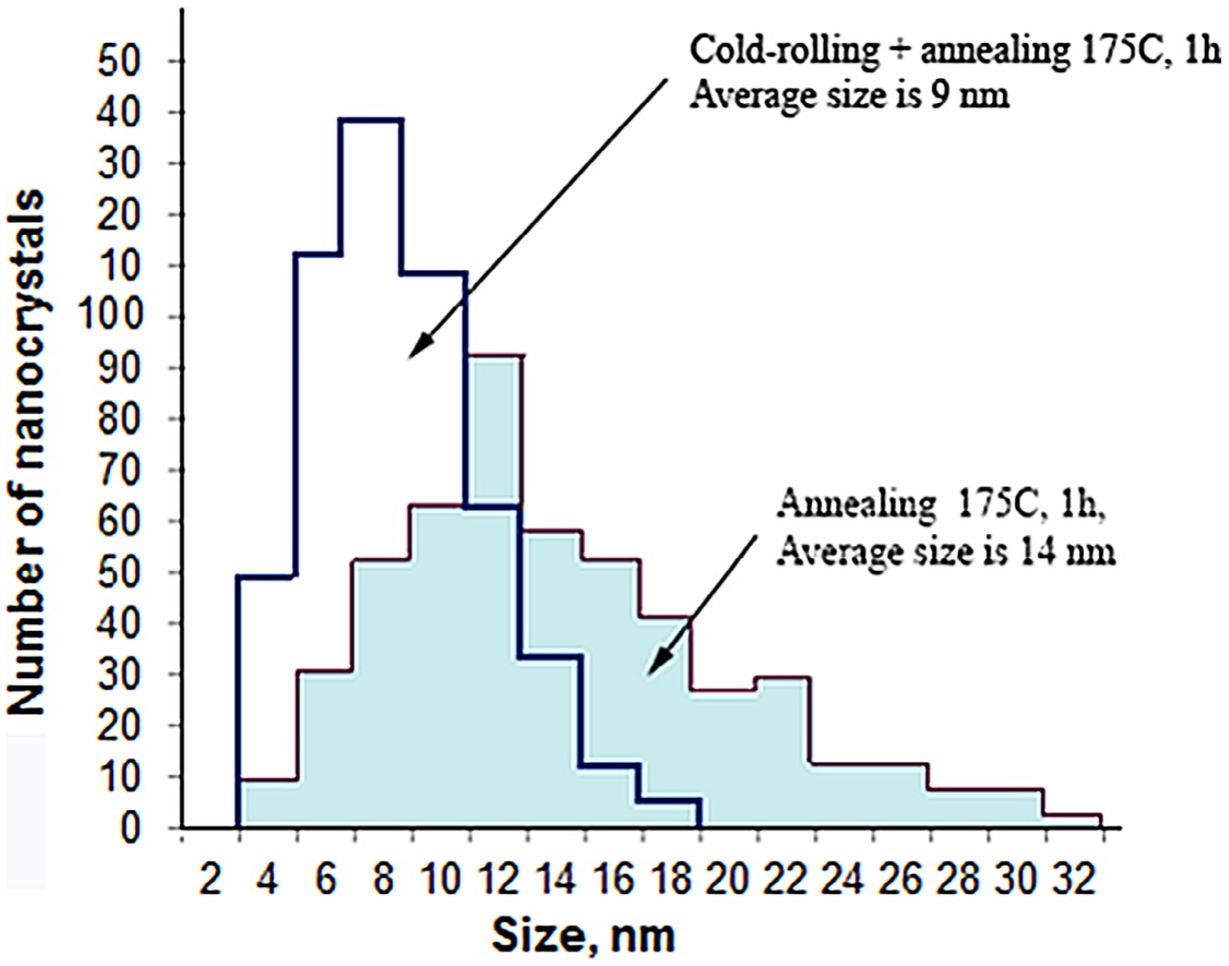

Fig. 19. Size distributions of nanocrystals in the samples subjected to annealing and combined treatment.

- parameters of external influences (temperature and duration of heat treatment, the type and level of the deformation, deformation temperature etc.);
- types of the treatment (using a combination of different types of influences).

For example, the combination of thermal and deformation treatments to alloys was shown to allow producing Al-based nanocrystalline materials with nanocrystals of diverse sizes and diverse nanocrystalline phase fractions.

ACKNOWLEDGEMENTS

The work was partially supported by the Russian Foundation for Basic Research (grants 13-02-00232, 14-42-03566, 14-43-03564).

Table 1. Nanocrystal sizes (*D*) and nanocrystalline phase fractions (*f*) after different types of treatment (HPT – high pressure torsion, HT – heat treatment, CR-cold rolling).

Treatment	Alloy	*D*, nm	*f*, %
HPT 1 rev	$Al_{87}Ni_8Gd_5$	6	22
HPT 5 revs	$Al_{87}Ni_8Gd_5$	6	25
HT (DSC)	$Al_{87}Ni_8Gd_5$	26	23
HT 175C 1h	$Al_{87}Ni_8Gd_5$	14	
CR + HT	$Al_{87}Ni_8Gd_5$	9	
HPT 1 rev	$Al_{87}Ni_8La_5$	11.4	15
HPT 5 revs	$Al_{87}Ni_8La_5$	12.8	17
HT	$Al_{87}Ni_8La_5$	32	12
CR + HT	$Al_{87}Ni_8La_5$	27	
HPT 0,1 rev	$Al_{90}Y_{10}$	9	24
HPT 1 rev	$Al_{90}Y_{10}$	9	30
HPT 2 revs	$Al_{90}Y_{10}$	9	40
HT	$Al_{88}Ni_{10}Y_2$	19	28
CR +HT	$Al_{88}Ni_{10}Y_2$	18	35
CR	$Al_{88}Ni_2Y_{10}$	~4	Few nanocrystals
HT	$Al_{88}Ni_2Y_{10}$	15	33
CR + HT	$Al_{88}Ni_2Y_{10}$	15	36
HT	$Al_{85}Ni_6Co_5Gd_6Si_1$	25-30 [30]	
CR	$Al_{85}Ni_6Co_5Gd_6Si_1$	10-15 [30]	
CR + HT	$Al_{85}Ni_6Co_5Gd_6Si_1$	20 [30]	

REFERENCES

[1] U. Köster, U. Schuheman, M. Blank-Bewersdorf, S. Brauer, M. Sutton and G.P. Stephenson // *Mater.Sci.Eng.* **A133** (1991) 611.

[2] K. Suzuki, A. Makino, A. Inoue and T. Masumoto // *Sci. Rep. RITU* **A39** (1994) 133.

[3] R.Z. Valiev, I.V. Alexandrov, Y.T. Zhu and T.C. Lowe // *J. Mater. Res*. **17** (2002) 5.

[4] T.G. Langdon // *Rev.Adv. Mater. Sci.* **31** (2012) 1.

[5] J. Eckert, M. Calin, P. Yu, L.C. Zhang, S. Scudino and C. Duhamel // *Rev. Adv. Mater. Sci.* **18** (2008) 169.

[6] Y.H. Kim, A. Inoue and T. Masumoto // *Mater. Trans. JIM* **32** (1991) 331.

[7] A.L. Greer // *Acta Metall.* **30** (1982) 171.

[8] D.V. Louzguine-Luzgin // *J. Alloys Comp.* **586** (2014) 52.

[9] G.E .Abrosimova, A.S. Aronin, E.Y.Ignat'eva and V.V. Molokanov // *JMMM* **2** (1999) 169.

[10] D.V. Louzguine and A. Inoue // *J.Non-Cryst. Solids* **311** (2002) 281.

[11] R. A.Andrievski and A. M. Glezer // *Physics-Uspekhi* **52** (2009) 315.

[12] A.L. Greer, Y.Q. Cheng and E. Ma // *Mater. Sci. Eng. R* **74** (2013) 71.

[13] G. Abrosimova, A. Aronin, D. Matveev and E. Pershina // *Mater. Lett.* **97 (**2013) 15.

[14] S. Hobor, A. Revesz, A.P. Zhilyaev and Zs. Kovacs // *Rev. Adv. Mater. Sci* **18** (2008) 590.

[15] E. Pershina, G. Abrosimova, A. Aronin, D. Matveev and V. Tkatch // *Mater. Lett.* **134** (2014) 60.

[16] D.V. Louzguine-Luzgin and A. Inoue // *J. Non-Crystalline Solids* **352** (2006) 3903.

[17] Zs. Kovács, P.Henits, S.Hobor and A.Révész // *Rev. Adv. Mater. Sci* **18** (2008) 593.

[18] P. Henits, Zs. Kovács and A. Révész // *Rev. Adv. Mater. Sci* **18** (2008) 597.

[19] A.N. Petrova, I.G.. Brodova, O.A. Plekhov, O.B. Naimark and E.V.Shorokov // *Technical Physics* **59** (2014) 989.

[20] G. E. Abrosimova, A. S. Aronin and S. V Dobatkin // *Physics of the Solid State* **49** (2007) 1034.

[21] G. E. Abrosimova, A. S. Aronin and Y.V.Kir'yanov // *Physics of the Solid State* **43** (2001) 2003.

[22] G. E. Abrosimova, A. S. Aronin and S. V Dobatkin // *J. of Metastable and nanocrystalline Materials series* **24-25** (2005) 69.

[23] A. Aronin, G. Abrosimova, D. Matveev and O. Rybchenko // *Rev. Adv. Mater. Sci.* **25** (2010) 52.

[24] G. E. Abrosimova, A. S. Aronin and I.I. Zverkova // *Physics of Metals and Metallography* **94** (2002) 102.

[25] G. E. Abrosimova and A. S. Aronin ***II*** *Physics of the Solid State* **50** (2008) 159.

[26] A.S. Aronin and G. E. Abrosimova // *Materials Letters* **83** (2012) 183.

[27] T. Langdon // *Rev. Adv. Mater. Sci*. **25** (2010) 11.

[28] C.-P. Chou and D. Turnbull // *J. Non-Cryst. Solids* **17** (1975) 169.

[29] H.S. Chen // *Mater. Sci. Eng*. **23** (1976) 151.

[30] L. Tanner and R. Ray // *Scr. Metall.* **11** (980) 783.

[31] A. Inoue, M. Yamamoto, H.M. Kimura and T. Masumoto // *J. Mater. Sci.* **6** (1987) 194.

[32] A.R. Yavari // *Acta Metall*. **36** (1988) 1863 .

[33] M. Marcus // *J. Non-Cryst. Solids.* **30** (1979) 317.

[34] H.S. Chen and D. Turnbull // *Acta Metal.* **17** (1969) 1021.

[35] M. Mehra, R. Schulz and W.L. Johnson // *J. Non-Crystall. Solids*. **61-62** (1984) 859.

[36] G.E. Abrosimova and A.S. Aronin // *J. Surface Investigation. X_ray, Synchrotron and Neutron Techniques* **9** (2015) 887.

[37] G.E. Abrosimova, A.S. Aronin, E.Yu. Ignat'eva and V.V. Molokanov // *JMMM* **203** (1999) 169.

[38] G.E. Abrosimova, A.S. Aronin and E.Yu. Ignat'eva // *Physics of the solid state* **48** (2006) 563.

[39] G.E. Abrosimova and A.S. Aronin // *Physics of the solid state* **40** (1998) 1603.

[40] G. Abrosimova, A. Aronin and A. Budchenko // *Mater. Letters* **139** (2015) 194.

[41] G. Abrosimova, A. Aronin and E. Ignatieva // *Mater. Sci. Eng. A* **449-451** (2007) 485.

[42] V.S.Pokatilov // *Doklady Akademii Nauk SSSR* **275** (1984) 79

[43] G.E. Abrosimova and A.S. Aronin // *Int. J. Rapid Solidif.* **6** (1991) 29.

[44] R. Stoering and H. Conrad // *Acta Metall* **17** (1969) 933.

[45] N. Mattern, G. Goerigk, U. Vainio, M.K. Miller, T. Gemming and J. Eckert // *Acta Materialia* **57** (2009) 903.

[46] N. Chen, D.V. Louzguine-Luzgin, G.Q. Xie, P. Sharma, J.H. Perepezko, M. Esashi, A.R. Yavari and A. Inoue // *Nanotechnology* **24 (**2013) 045610.

[47] H.Gleiter // *Mater. Science Forum* **584-586** (2008) 41.
[48] D. Şopu, K. Albe and Y. Ritter // *Appl. Phys. Letters* **94 (**2009) 191911.
[49] M. Ghafari, S. Kohara and H. Hahn // *Appl. Phys. Letters* **100** (2012) 133111.
[50] N. Chen, R. Frank, N. Asao and D.V. Louzguine-Luzgin // *Acta Mater*. **59** (2011) 6433.
[51] J.H. Han, N. Mattern, U. Vainio and A. Shariq // *Acta Mater.* **66** (2014) 262.
[52] G.E. Abrosimova, A.S. Aronin, A.V.Bezrukov, S.P.Pankratov and A.V.Serebryakov // *Physics of Metals* **4**(1982) 114
[53] H.H. Liebermann, C.D.Jr. Graham and P.J. Flanders // *IEEE.Trans. Magn*. **13** (1977) 1541.
[54] G.E. Abrosimova, A.V.Serebryakov and Zh.D.Sokolovskaya // *Fizika metallov I metallovedenie* **66** (1988) 727
[55] G.E. Abrosimova, A.P. Zhukov and B.K. Ponomarev // *Phys. Stat. Sol*. **111a** (1989 K237.
[56] H. S. Chen // *Sci. Eng*. **33** (1976) 151.
[57] J.L. Walter, F. Bacon and F.E. Luborsky // *Mater. Sci. Eng.* **24** (1976) 239.
[58] Y. Waseda, *The structure of liquids, amorphous solids and solid fast ion conductors* (Pergamon Press, 1981).
[59] C.A. Pampillo and H.S // *Mater. Sci. Eng.* **13** (1974) 181.
[60] C.A . Pampillo // *J. Mater. Sci.* **10** (1975) 1194.
[61] Q.S. Zeng // Proc. Nat. Acad. Sci. USA. **104(34)** (2007) 13565.
[62] A. Naudon // *J. Non-Crystalline Solids* **61/62** (1984) 355.
[63] X.D. Wang, J. Bednarcik, K. Saksi, H. Franz, Q.P. Cao and J.Z. Jiang // *Appl. Phys. Lett.* **91** (2007) 081913.
[64] M. Stoica, J. Das, J. Bednarcik, H. Franz, N. Mattern, W.H. Wang and J. Eckert // *J. Appl. Phys.* **104** (2008) 013522.
[65] X.D. Wang, J. Bednarcik, H. Franz, H.B. Lou, Z.H. He, Q.P.Cao and J.A.Jiang // *Appl. Phys. Lett.* **94** (2009) 011911.
[66] G.E. Abrosimova, A.S. Aronin, N.S. Afonikova and N.P. Kobelev // *Physics of Solid State* **52** (2010) 1892.
[67] D.P. Shirnina, G.E. Abrosimova and A.S. Aronin // *Design Materials Technology* **3(18)** (2011) 80.
[68] Y. Yokoyama, T. Yamasaki and A. Inoue // *Rev. Adv. Mater. Sci.* **18** (2008) 131
[69] H. Gleiter // *Prog. Mater. Sci.* **33** (1989) 223.
[70] R. Birringer // *Mater. Sci. Eng*. **A117** (1989) 33
[71] N. Wang, Z. Wang, K.T. Aust and U. Erb // *Acta Metall. Mater.* **43** (1995) 519.
[72] R.Z. Valiev, *Nanomaterials by Severe Plastic Deformatio*, ed. by M.J. Zehetbuuer (WILEY: Vienna, 2002)
[73] A.L.Greer, In: *12th International Conference on Rapidly Quenched and Metastable Materials* (Dresden, 2008), Rq12.
[74] R. Maass, D. Klaumunzer and J.F.Lofler // *Acta Mater.* **59** (2011) 3205.
[75] E.O. Hall // *Proc. Phys. Soc. London Sect*. **B64** (1951) 747.
[76] N.J. Petch // *J. Iron Steel Inst.* **174** (1953) 2
[77] K. Lu // *Mater. Sci. Eng*. **R16** (1996) 161.
[78] X.D. Liu, J.T. Wang and B.Z.Ding // *Scripta Met.Mater*. **28** (1993) 59
[79] V.A. Pozdnyakov // *Physics of Metals and Metallography* **97** (2004) 7
[80] A.M. Glezer, S.E. Manaenkov and I.E. Permyakova // *Bulletin of the Russian Academy of Sciences* **71** (2007) 1702.
[81] A.M. Glezer, S.V. Dobatkin and M.R. Plotnikova // *Materials Science Forum* **584-586** (2008) 227.
[82] J. Latuch, A. Kokoszkiewicz and H. Matyja // *Mater. Sci. Eng*. **A226-228** (1997) 809.
[83] M.A. Munoz-Morris, S. Surinach, M.D. Baro and D.G. Morris // *Mater.Sci. Eng*. **A375-377** (2004) 965.
[84] A. Inoue, Y. Horio, Y.H. Kim and T. Masumoto // *Mater.Trans. JIM* **33** (1992) 669.
[85] A.A.Rusakov, *X-ray Diffraction in Metals* (Atomizdat: Moscow, 1977), In Russian.
[86] G.E. Abrosimova, A.S. Aronin and N.N. Kholstinina // *Physics of the Solid State* **52** (2010) 445.
[87] G. E. Abrosimova and A. S.Aronin // *Physics of the Solid State* **44** (2002) 1003.
[88] G. E. Abrosimova and A. S.Aronin // *Physics of the Solid State* **51** (2009) 1765.
[89] J. Pan, Q. Chen, L. Liu and Y. Li // *Acta Materialia* **59** (2011) 5146.
[90] G. Abrosimova, A. Aronin, O. Barkalov, D. Matveev, O. Rybchenko, V. Maslov and V. Tkatch // *Physics of Solid State* **53** (2011) 229.